Contribution of Paleosol Stratigraphy to Geotechnical Modeling: A Case Study of the Two Towers in Bologna

Contribution of paleosol stratigraphy to geotechnical modelling: the case study of the Two Towers in Bologna

Marchi Michela[1], Bertolini Ilaria[2], Bruno Luigi[3] Amorosi Alessandro[4] and Gottardi Gottardi[5]

[1.] *DICAM Department, University of Bologna, Viale del Risorgimento 2, - 40136, Bologna (BO), Italy (corresponding author). E-mail: michela.marchi@unibo.it*

[2.] *DICAM Department, University of Bologna, Viale del Risorgimento 2, - 40136, Bologna (BO), Italy. E-mail: ilaria.bertolini3@unibo.it*

[3.] *Department of Chemical and Geological Sciences, University of Modena and Reggio Emilia, Via Giuseppe Campi 103 - 41125 Modena (MO), Italy. E-mail: luigi.bruno@unimore.it*

[4.] *Department of Biological, Geological and Environmental Sciences, University of Bologna, Piazza di Porta San Donato 1 - 40136, Bologna (BO), Italy. E-mail: alessandro.amorosi@unibo.it*

[5.] *DICAM Department, University of Bologna, Viale del Risorgimento 2, - 40136, Bologna (BO), Italy. E-mail: guido.gottardi2@unibo.it*

ABSTRACT

Paleosol identification is a valuable tool for stratigraphic correlation in fine-grained alluvial successions, applicable at both local and regional scales. This study investigates paleosol formation and their key physical properties, focusing on pedogenic processes affecting soil mechanical behaviour. A methodology is developed for identifying paleosol horizons using common in situ tests, particularly CPT, facilitating the transition from a paleosol-based stratigraphic model to a geotechnical-stratigraphic one, for engineering applications. This approach is applied to data from the historic center of Bologna, including the Asinelli and Garisenda Towers, two medieval structures founded on fine-grained alluvial deposits. Radiocarbon-dated paleosols from the Late Pleistocene in this area show increased strength and stiffness, as revealed by in situ testing, likely attributed to cementation and aging. Comparing borehole data with CPT enabled the identification of weakly developed paleosols (Inceptisols), enhancing geotechnical model accuracy. The paleosol-based stratigraphic model presented in this study provides critical information for developing a refined geotechnical model that can account for even subtle variations in microstructure, features often overlooked by conventional CPT-based and core-based soil profiling methods and highlights significant subsurface settlements experienced by the Two Towers over time. This research demonstrates the effectiveness of the proposed interdisciplinary approach, emphasizing the potential of paleosol identification for engineering applications in complex subsurface environments.

Keywords: fine-grained alluvial sediments; paleosol stratigraphy; in situ testing (CPT); settlements of historic foundations; microstructured soils.

1 Introduction

Depositional and post-depositional processes, collectively known as geological history, profoundly influence the soil structure which in turn affects its mechanical behaviour (Schmertmann, 1991; Ltifi et al., 2014; Cruz et al., 2012; El Howayek et al., 2017; Berisavljević et al., 2019). The term “structure”, or the other commonly adopted “microstructure”, refers to the combination of fabric—the arrangement of the soil particles—and bonding, which includes interparticle forces beyond simple frictional interactions (Lambe & Whitman, 1969). In general, all soils exhibit some degree of structure, whose intensity depends on the processes that have affected the soil throughout its geological history. The most pronounced structural features typically result from post-depositional processes such as unloading, aging, cementation, thixotropy, cold welding and their combinations. Conversely, reconstituted soils, which have undergone complete remolding (defined as de-structuration, according to Leroueil & Hight (2003)), exhibit the least pronounced microstructure (Burland, 1990). Natural clays, normally to lightly overconsolidated and uncemented, develop microstructure primarily during one-dimensional virgin compression. Throughout this paper, the terms “microstructured soils” and “structurally bonded soils” are adopted to describe soils that exhibit different mechanical characteristics compared to “ideal soils” (i.e., recent – of Holocene to Pleistocene origin - and normally consolidated, unbonded soils), in accordance with the definition given by Robertson (2015). For the sake of clarity, the terminology “structured and unstructured soil” can also be found in the literature with the same meanings.

In fine-grained successions, field investigations often reveal layers affected by post-depositional phenomena, clearly indicated by changes in soil response not explained by variations in lithology or soil texture. In geotechnical engineering practice, such conditions are often oversimplified and qualitatively attributed to surface exposure, leading to descriptions such as "drying crusts" (Burland, 1990; Leroueil & Hight, 2003), without a rigorous characterization. “Drying crusts” are structurally bonded soils typically resulting from exposure-related processes, which modify the soil structure after deposition. Among these processes, desiccation driven by evapotranspiration leads to soil shrinkage, fracturing, increased matric suction, and generally an overall enhancement of mechanical properties. Chemical precipitation, induced by rainfall water percolation in soils under suitable pH, temperature, CO_2 concentration and mineral availability, generates soil interparticle bondings at the microstructural level. When calcite is the precipitating mineral, this process is referred to as cementation.

Drying crusts often exhibit mechanical behaviour similar to that of overconsolidated soils. However, they are not truly overconsolidated in the classical geotechnical sense. Unlike mechanically overconsolidated soils—which have experienced effective vertical stresses greater than the current overburden at the time of sampling, the elevated values of overconsolidation ratio (OCR) observed in microstructured soils should be interpreted as apparent overconsolidation. This condition arises from microstructure modification —such as interparticle bonding and cementation— and matric suction generated by surface tension at the air-water interface in (partially saturated) soil pores, rather than from a true unloading-reloading stress history due to erosion or mass redistribution (Yenes et al., 2020).

The recognition and lateral tracing of pedogenized horizons (paleosols) within sedimentary successions with limited textural variations is common in paleosol stratigraphy (McCarthy & Plint, 2003). The differentiation of these horizons from overlying and underlying sediments is not related to environmental changes during deposition, but to modifications occurred during prolonged phases of subaerial exposure after deposition. However, paleosols are frequently overlooked in geotechnical models, and their distinctive mechanical characteristics are not explicitly attributed to the post-depositional processes that generated them, often being considered localized heterogeneities within relatively uniform stratigraphic units.

Geological models have made significant advances in reconstructing the three-dimensional depositional architecture of subsurface deposits by integrating stratigraphic data from boreholes with geophysical and surface analyses, even in complex alluvial successions (Salvany & Aguirre, 2020, Giacomelli et al., 2023). At the same time, geotechnical models are improving the interpretation of in situ tests, focusing mainly on conventional ideal soils. However, soils affected by pedogenic processes (e.g., aging and cementation) are well documented in the stratigraphic literature (Robertson, 2016; Tentori et al., 2022; Campo et al., 2023; Baruffardi et al., 2025), however, their explicit integration into geotechnical models remains at an early stage, often due to the limited integration between stratigraphic-sedimentological and geotechnical disciplines. A step forward would require combining the stratigraphic characterization of soils with geotechnical expertise based on soil mechanical response.

This study aims to bridge the gap between purely geotechnical and geological approaches, offering an integrated methodology for the development of refined geotechnical-stratigraphic models in complex alluvial settings, through the combination of cone penetration testing and high-resolution paleosol stratigraphy. A

specific objective is to guide the identification of paleosols and their internal horizons through the analysis of trends and attained values of key CPT-derived geotechnical parameters, an essential procedure in cases where sedimentological information is limited or lacking.

The proposed methodology has been developed using data from the subsoil of the Bologna Two Towers, where paleosols not only served as support for geotechnical analysis but also offered insights into an important engineering application: estimating the cumulate settlements beneath the Two Towers over the course of centuries.

This study integrates techniques and methods from different disciplines, including geotechnics, stratigraphy and pedology. Given the distinct terminologies used in these fields, and the potential for overlapping terms with different meanings, an initial lexical clarification is necessary. The word 'soil' is defined in pedology as a natural body that occurs on the land surface, composed of solids, liquid, and gases, and characterized by horizons that are distinguishable from the initial material as a result of additions, losses, transfers, and transformations of energy and matter or by the ability to support rooted plants in a natural environment (Soil Survey Staff, 1999). The processes occurring in soil lead to a modification of the initial sediment (or rock) and are known as pedogenesis. Based on this definition, paleosols are defined in stratigraphy as fossil soils—former surface sediments that underwent pedogenic development during subaerial exposure and were subsequently buried by younger deposited material, thereby becoming isolated from active soil-forming processes (Johnson, 1998).

In geotechnical engineering, the term soil generally refers, without distinction, to the unbonded granular material covering the Earth's surface, which can be excavated using hand tools, distinct from rocks. This geotechnical definition is used throughout the manuscript, except for subsection (2.1) in which soil refers to its pedological meaning, denoting material originally derived from sediment but subsequently altered over time by pedogenic processes.

2 Multiple paleosol profiles: mechanisms of formation and features

2.1 Formation of multiple soil sequences in subsiding alluvial settings

Multiple paleosol profiles have been documented in the subsurface of subsiding alluvial plains worldwide (Tsatskin et al., 2015; Srivastava et al. 2018; Bertolini et al., 2022b). In these settings, subsidence continuously creates space for sediment deposition, with soil development and burial closely linked to fluvial activity, which

117 can be influenced by a variety of factors (Demko et al., 2004). The ratio between sediment supply and river
118 discharge is a key parameter that controls fluvial activity. A possible mechanism of multiple soil formation in
119 a well-drained floodplain environment is illustrated below (Fig. 1), with specific reference to Inceptisols (Soil
120 Survey Staff, 2014), such those observed beneath the Two Towers (Bruno et al., 2020).

121 Phase 1: **SOIL DEVELOPMENT** - Low sediment supply/discharge may lead to river entrenchment.
122 Consequently, (i) interfluvial areas are subaerially exposed and protected by fluvial sedimentation, and (ii)
123 groundwater table is lowered. Due to rain-water percolation in the vadose zone, carbonates are leached from
124 the topsoil (A_b horizon), and precipitated a few decimeters below in the B_k horizon. Organic matter introduced
125 in the topsoil from vegetation is rapidly oxidized and decomposed. Soil weathering due to pedogenic processes
126 decreases with depth and is weak in the B_w horizon, while absent in the C horizon. The topsoil exposed to
127 subaerial conditions assumes a darker colour (A_b horizon) due to accumulation and decomposition of organic
128 material, and to carbonate leaching. Owing to carbonates precipitation, the underlying B_k horizon is
129 characterized, instead, by a whitish colour, abundant carbonate concretions and cementation. Due to their
130 distinctive features (including dark-whitish colour couplets) and considerable lateral continuity, paleosols play
131 a fundamental role in the reconstruction of the stratigraphic architecture of interfluvial, fine-grained
132 successions (McCarthy & Plint, 2003).

133 Phase 2: **SOIL BURIAL** (i.e. PALEOSOL FORMATION) - When external factors (e.g. climate changes)
134 increase the sediment supply/discharge ratio, fluvial incisions are rapidly filled and rivers enter in a phase of
135 metastable equilibrium, characterized by frequent flooding events and crevassing. As a consequence, soils
136 developed in interfluvial areas are progressively buried under a pile of sediments. During this phase, pedogenic
137 processes, such as carbonate leaching and transfer to the deeper soil horizons, are hindered by: (i) continuous
138 sediment supply to interfluvial areas; (ii) raised groundwater table and the lack of a vadose zone. Pedogenic
139 processes are interrupted since burial, and the fossilized soil turns into a paleosol.

140 Phase 3: **RENEWED SOIL DEVELOPMENT** - If boundary conditions permit a new phase of fluvial
141 incision, a new soil profile develops above the former one. If the pile of sediment is sufficiently thin, and
142 sediment is exposed for long periods, the buried soil can be partly involved in the new pedogenic cycle (e.g.
143 leached carbonate can precipitate into the buried A_b horizon) or totally overprinted by the new soil. If, on the

contrary, the new soil develops on a sufficiently thick sediment package, the buried soil (i.e. the paleosol) will be preserved.

2.2 Pedogenic processes affecting soil mechanical behaviour

Physical and chemical alterations of the soil microstructure can result from pedogenic modifications. Cementation and aging are the main processes that affect the microstructure of buried soils (e.g.; McCarthy & Plint, 1998; Srivastava et al., 2018; Tentori et al., 2022; Hauser et al., 2025).

Cementation is the result of the deposition of secondary calcite in form of carbonate nodules and filaments. Carbonate in the sediment may undergo a leaching process in the topsoil that weakens the skeleton by forming cavities or voids, while enriching the underlying horizon with distinct degrees of cementation: from weak particle bonding that could be easily broken (weak cementation) to a completely solidified matrix (strong cementation). Carbonates are extremely sensitive to pedogenic processes. Since these processes vary spatially—especially with depth—they may result in pronounced vertical variability in soil mechanical properties (Demars, 1982). For this reason, the alternation of cemented and uncemented layers is extremely common. The presence of structurally bonded soils (i.e., "microstructured soils") generally suggests an enhancement in mechanical behaviour that could not be explained by void ratio or stress history alone (Leroueil & Hight, 2003; Robertson, 2009). Compared to ideal (i.e., young and unstructured) soils under the same initial conditions of void ratio and stress state, structurally bonded soils exhibit higher yield stress, peak of strength and small-strain stiffness (Leroueil, 1992; Cotecchia & Chandler, 1997; Rampello & Viggiani, 2001). By definition, soils become "destructured'' when cementing bonds are partly or entirely broken and this condition is linked to a general degradation in mechanical properties (Amorosi & Rampello, 1998; Leroueil & Hight, 2003). Thus, the soil microstructure, stress history and void ratio are equally important in the description of natural fine-grained deposits (Leroueil & Vaughan, 1990).

The general term "aging" includes the effects of "pure aging", as well as those caused by the subaerial exposure of soils to a variety of processes (chemical weathering, swelling-desiccation, freezing-thawing, modification of the water table, among others) (Schmertmann, 1991). The term "pure aging" refers to processes that involve only time-dependent changes: soils age with time and an enhancement of soil properties is generally registered (Mitchell & Soga, 2005). Nonetheless, Mitchell (1986), Schmertmann (1991) and Baxter & Mitchell (2004) documented soils where aging led to a deterioration of some of their properties.

All processes that constitute aging act simultaneously. Separation of their different effects on soil mechanical behaviour can be challenging, especially outside the controlled environment of laboratory testing, where processes may act simultaneously or over different time scales. “Pure aging” affects soil horizons (A_b, B_k and B_w) proportionally to the elapsed time interval between deposition and soil testing, while the overall effects of aging are typically heterogeneous with depth.

A combination of the two aging mechanisms can produce significant modifications in soil properties. A general enhancement of mechanical parameters due to aging has been widely investigated and recognized, both on material strength (Mitchell & Soga, 2005; among others) and stiffness (Curzi et al. 2017; among others). In addition, hydraulic permeability usually decreases due to micro-organisms growth, void reduction by creep or by very fine particles filling (Dunn & Mitchell, 1984; Ltifi et al, 2014). Such modifications in soil properties can show horizontal heterogeneity also in relatively uniform deposits. “Aging”, unlike “pure aging”, is deeply affected by local variations of boundary conditions, such as rainfall percolation, water ponding, temperature, and solar exposure, among others.

3. Materials and methods

The subsequent subsections 3.1 and 3.2, together with Figs. 2 A and B, illustrate the step-by-step procedure of analysis, from paleosol identification to the integration of geotechnical data, essential for constructing geotechnical-stratigraphic models of a paleosol-bearing succession.

3.1 Paleosol identification through sedimentological analysis

The first step is the sedimentological description of soil cores, which is mainly based on standard classification practices (UNI EN ISO 14688-1, 2018). In this phase, soil texture estimates, soil colour, and the presence of accessory materials (e.g., vegetal remains, macrofossils, carbonate concretions) are reported. Quick tests, such as the pocket penetrometer, torvane, and reaction to hydrochloric acid, are typically used on sediment cores to quickly assess their properties. All these features are considered for the recognition of paleosol horizons A_b, B_k and B_w (Soil Survey Staff, 2014).

Key characteristics of the **A_b horizon** include a dark-brown colour due to a relatively high organic content and low carbonate content (see Fig. 2 C), and relatively high values of undrained shear strength, measured with handheld torvane and pocket penetrometer. These rapid assessments of undrained shear strength are intended primarily for comparative purposes between different horizons. Typically, no visible reaction to dilute

hydrochloric acid (10%) is shown by this horizon, due to its almost-complete carbonate leaching. The **B_k horizon** is notably identified by a yellowish-brown/light-brown colour and abundance of nodules of secondary calcite. The interface between A_b and B_k horizons shows the highest values of undrained shear strength, as measured by quick field tests. A progressive decrease of undrained shear strength is observed downward. This is a consequence of post-depositional processes: the interface and the uppermost centimetres of the B_k horizon show the highest degree of cementation and abundance of carbonate nodules. Highly visible reaction to hydrochloric acid is shown by this horizon, due to its remarkable carbonate content. Occasionally, carbonate nodules have cm size (Fig. 2 D). More often, they are small (mm size) or not detectable by visual inspection. The **B_w horizon** is characterized by a yellowish-brown/greyish-brown colour and lower undrained shear strength, obtained by handheld torvane and pocket penetrometer, compared to the B_k horizon. Cementation due to pedogenic processes is minimal. For the **C horizon**, the main distinctive features are a yellowish-brown/greyish-brown colour, as for the B_w horizon, and a lack of cementation due to pedogenesis. Nevertheless, the post-depositional history of this horizon can be affected by "pure aging" acting over time. The lowest values of undrained shear strength are obtained from this horizon through quick field tests.

In some cases, distinguishing horizons A_b, B_k, B_w and C can be challenging. This is the case of closely-spaced paleosols affected by knock-on pedogenic processes. For instance, buried A_b horizons may undergo re-carbonation due to pedogenesis of overlying layers. Moreover, when the sediment deposited during an alluvial phase has reduced thickness (< 3 m), pedogenesis may affect the entire deposit, leading to the absence of the C horizon.

These characteristics form the foundation for the paleosol identification methodology, which will be further detailed in the following sections. In practice, paleosol stratigraphy first relies on core observations to identify the distinctive soil horizons, as described above. When visual inspection alone is insufficient, specific laboratory tests are recommended to accurately identify paleosol horizons, as outlined by Bruno et al. (2020). To this scope, the most effective laboratory tests are:

- *organic content* determination: it is used to identify A_b horizons, which display the highest values.

- *carbonate content* determination: this information is particularly useful in the distinction between B_k and B_w.

- *particle-size distribution* analysis: it is useful for the distinction between A_b and B_k.

- *Plasticity Index* (PI) determination: being characterized by higher clay content, the A_b horizon shows higher PI than underlying B horizons.

Radiocarbon dating tests on samples from the A_b horizon can be used in the stratigraphic correlation of Late Pleistocene and Holocene paleosols over large areas (Scarciglia et al., 2023). These tests measure the decay of the radioactive isotope of carbon (^{14}C) stored in the organic material, which provides the age of a specimen. Therefore, such measurements can hardly be carried out on B_k and B_w due to their low organic content.

An additional methodology that could notably improve the characterization of paleosol horizons, is the micromorphological analysis, based on the microscopic observation of thin sections from undisturbed soil samples. This technique allows for the investigation of soil microstructure, including particle morphology, fabric, interparticle bonding, void distribution, and other features across different horizons (Srivastava et al., 2018; Tentori et al., 2022).

3.2 Geotechnical-stratigraphic model and In Situ Testing

In alluvial contexts, where geological analysis reveals the presence of paleosol-bearing successions, a step-by-step procedure can be used to develop a refined geotechnical-stratigraphic model, as outlined in the workflow of Fig. 2 B and summarized below:

1. Perform no fewer than three closely spaced tests to mitigate the effects of potential soil heterogeneity. These should include at least one continuous coring borehole, one cone penetration test CPT, and a s-wave logging test (e.g., Downhole or Crosshole).
2. Combine the CPT and seismic test data to identify depth intervals where the modified normalized small-strain rigidity index (K_G*) (defined in Table 1) exceeds the threshold value (> 330), which indicates the potential presence of structurally bonded soils.
3. At these identified depths, conduct targeted physical characterization tests and perform a detailed visual inspection of sediment cores. Apply the methodology proposed in the previous subsection (2.1) and schematized in Fig. 1 A to establish the local paleosol stratigraphy, identifying the depth intervals and distinctive horizons of each paleosol. Radiocarbon dating of paleosol horizons can provide valuable supporting evidence. Thin layers or horizons (approximately less than three times the piezocone diameter) should be excluded from this analysis, as their characteristics may not be clearly detectable in subsequent CPT interpretations.

4. Develop the local geotechnical-stratigraphic model by analyzing the normalized Soil Behaviour Type (SBT_n) profile derived from the CPT interpretation according to Robertson (2009), alongside the paleosol stratigraphy. Divide the deposit into homogeneous units based on soil maturity and behaviour.
5. This procedure can be extended to the entire investigation area by performing CPT tests alone. Paleosols identified from closely-spaced data (point 4) serve as reference markers for analyzing scattered CPT.
6. To verify lateral paleosol tracing, additional scattered corings should be performed, and the paleosol stratigraphy updated following the workflow in Fig. 2 A.

The guidelines for identifying pedogenised horizons in CPT tests, as required in points 4 and 5 of this procedure, have been developed in the following sections with reference to the case study and represent one of the novel contributions of this work.

4 The Two Towers site: geologic context; hydrologic setting and field investigations

The investigation site, covering approximately 1500 m², is located in the Bologna's city center, in Ravegnana Square (Fig. 3 A), around the Asinelli and Garisenda Towers (Fig. 3 B). Built between the 12th and 13th centuries, these towers are among the 22 remaining out of an original 75 and are key landmarks of the city (Bertolini et al., 2022a). This study focuses on the shallow stratigraphy as part of the geotechnical model for soil-structure interaction analysis. Bologna is situated at the southern margin of the Po Plain. Two main rivers, Reno and Savena, flowing west and east of the town (red areas in Fig. 4 A), respectively, deposited hundreds of meters thick multi-storey fluvial gravel bodies (Amorosi et al., 2014). These gravel bodies, typically amalgamated in proximal areas, grade distally into alternations of gravel bodies with overbank fine-grained horizons (orange area in Fig. 4 A; see also Figs. 4 B and C). Underneath the historic centre of Bologna (within the grey square in Fig. 4 A) coarse-grained deposits are rare and show limited lateral continuity. Silty-clay and clayey-silt material is dominant up to a considerable depth (Bruno et al., 2020; Giacomelli et al. 2023). The prevalence of fine-grained sediments in the Bologna subsoil suggests deposition in low-energy interfluvial environments. Small creeks (e.g. Meloncello, Ravone, Aposa) with torrential regimes (< 10 km length) draining small sectors (< 20 km²) of the Apennine foothills feed this area. Subsurface stratigraphy is characterized by a series of paleosols formed during phases of subaerial exposure, alternating with depositional

events during the Middle and Late Pleistocene (Amorosi et al., 2014). Structural and geotechnical studies on the towers and foundations, conducted since the early 20th century, aim to inform preservation strategies (Marchi et al., 2019; Bertolini et al., 2022a, Marchi et al., 2022).

Four investigation campaigns (1973–75, 1995, 2000–2009, and 2016) included boreholes, laboratory tests on soil samples (with identification of the main physical properties), piezometric monitoring, CPTs, and DMTs (Fig. 5). These investigations consistently recorded a water table at an average depth of 5.6 m, with seasonal oscillations of less than 90 cm, and a hydrostatic pore pressure regime within the upper 20 m of the soil profile (Marchi et al., 2022). The 2016 campaign data, combined with earlier campaigns, informed the development of a paleosol-based stratigraphic model (Fig. 6) along cross-section Z-Z' (the trace is reported in Fig. 5 B), as detailed in the next section. High-resolution CPT data was crucial in identifying horizon boundaries within paleosol successions, enabling the construction of a detailed geotechnical-stratigraphic model for the site.

5 Paleosol-based stratigraphic model and physical characterization of paleosols

The most common paleosols in the investigated area are Inceptisols (Soil Survey Staff, 2014), weakly developed paleosols characterized by a well-defined horizon succession consisting of A_b (buried A horizon), B_k (calcic – carbonate enriched – B horizon) and locally B_w (cambic - weakly developed - B horizon). These paleosols formed under subaerial exposure lasting approximately 3-5 thousand years (Bruno et al., 2022). Inceptisols beneath the Two Towers developed during the last glacial period, between ca. 80,000 and 11,700 years ago (Bruno et al., 2020). The stratigraphic correlation of paleosols developed in the last 50000 years is supported by 14 radiocarbon dates (red dots in Fig. 6).

Following Amorosi et al. (2014), four Inceptisols, dating back to the Late Pleistocene, were identified and named, from the deepest to the shallowest, P1, P2, P3 and PH. Paleosol PH marks the boundary between Upper Pleistocene and Holocene deposits. For the construction of the foundation systems of the Garisenda and Asinelli towers, most of the Holocene succession above ~4.5 m of depth was removed (Fig. 6). Nonetheless, two Holocene paleosols overlying PH are still visible in borehole SPZ100. Radiocarbon dates from core SDH1 show that paleosol PH was exposed for a few millennia during the Early Holocene. The overall paleosol thickness, the thickness of individual horizons, and the sequence of horizons defining paleosols P1, P2, P3 and PH are summarized in Table 2.

Results of laboratory tests executed on samples from the four paleosols (P1 to PH) are shown in Figs. 7 and 8. The results of these tests were used to refine the paleosol stratigraphy shown in Fig. 6 and to characterize paleosol horizons. Atterberg Limits were determined and plotted on the Casagrande Plasticity Chart, as shown in Fig. 7. The majority of the A_b samples are positioned on or above the A-Line, resulting in CH samples typically defined as inorganic clays, fat clays with high plasticity (Fig. 7 A), while B_k and B_w samples are located on or above the A-Line in the Medium-Low plasticity area (Fig. 7 B and C, respectively). These results are consistent with the higher plasticity and clay content of the A_b samples compared to those of B_k and B_w, due to continuous mineralization of the organic material (i.e., process of decomposition of the organic matter into simpler inorganic substances) and its association with clay minerals (Yandong et al., 2018). Figure 8 shows four soil texture triangles of samples belonging to the three horizons. The size of the dots is proportional to the PI values (in graph B), to the organic content (in graph C) and to the carbonate content (in graph D). Samples from A_b horizons (red points) are characterized by high clay and silt content (average values ~39% and ~49%, respectively), and a low proportion of sand (~9%). Conversely, samples from B_k and B_w horizons (blue and green dots) show lower clay content (~29 and 25%, respectively) and higher silt content (~51 and 58%) than in A_b (value ranges reported in Table 3). The higher proportion of sand in B_k and B_w samples is ascribable to soil carbonatation that enriched their matrix in carbonate nodules, whose dimensions fall between coarse-silt and sand.

In graph B of Fig. 8, PI values are combined with textural information. The larger dimension of the red dots suggests higher plasticity of A_b samples (29%), compared to B_k and B_w. In graph C, the organic content is combined with soil textural characteristics. As expected, samples from A_b show the highest values of organic matter (average 2.5%), compared to B_k and B_w (1.7% and 1.6%, respectively). In Graph D, the carbonate content is combined with soil texture. The carbonate content is particularly low along the A_b horizons (average ~6.5%), suggesting leaching of carbonates from the topsoil during exposure and precipitation in the underlying horizons B_k and B_w (average ~26% for both). These trends are consistent with the geochemical characterization of coeval Inceptisols from the Po Plain, which invariably showed patterns of calcium mobilization from surface A horizons through leaching and accumulation in the underneath B horizons (Amorosi et al., 2021).

6 Geotechnical-stratigraphic model of the subsoil beneath the Two Towers

The geotechnical model of the Two Towers area is supported by the previously defined paleosol-based stratigraphic model (Fig. 6), along with the results of in situ tests (as outlined in Fig. 2 B). For this purpose CPT1 (location shown in Fig. 5) was analysed first, as this test is associated with a continuous core, for which detailed stratigraphic analysis is available (SDH1), together with a Downhole P- and S-wave logging in accordance with ASTM D7400M-19 in hole SDH1.

6.1 CPT data interpretation

The application of Robertson's (2009) SBT_n chart is typically in agreement with USCS-based classification for normally consolidated (NC), young, unbonded soils and for most soils with a light bonded microstructure. However, extreme care is recommended when applied in presence of soils characterized by a remarkable post-depositional history (Robertson, 2009). Since the investigated deposit appears to have a light to medium bonded microstructure, the application of Robertson's (2009) classification system to CPT1 data was not trivial and is consistent with the presence of a relatively uniform succession of fine-grained soils underneath a 4.5 m thick layer of anthropogenic fill. In fact, the SBT_n profile (Fig. 9), represented together with the outcome of the nearest borehole, SDH1, shows clustering of data points almost exclusively in classes 3 and 4 (i.e. clay and silt mixtures).

Despite relatively uniform textural characteristics of the deposit, the vertical profiles of the main geotechnical properties (e.g., OCR and s_u profiles in Fig. 9) obtained through the correlations reported in Table 1 show a significant dispersion, possibly as a result of microstructuration and aging (Saye et al., 2013).

The presence of a significant microstructure in soils can be detected through the definition of the modified normalized small-strain rigidity index, K_G*, whose formulation is reported in Table 1 (Ku & Mayne, 2013; Roberson, 2016). Following this approach, soils with a K_G* value exceeding 330 are classified as possibly structurally bonded soil ("microstructured soil").

For the analysed case study, the v_s-profile derived from Downhole seismic test conducted in borehole SDH1 (location in Fig. 5 B) was used to determine G_0 for the K_G* calculation.

The quantification of K_G* for CPT1 is shown in the last column of Fig. 9.

Initially, **four main geotechnical units** (R, U1, U2 and U3 in Fig. 9) were identified primarily on the basis of the SBT_n profile . U1 is a succession of uniform layers with considerable (but variable) thickness belonging to SBT classes 3 or 4. In contrast, U2 is a dense intercalation of thin layers of SBT 3 and 4. Underneath U2, unit

U3 appears to be quite homogeneous, with a continuous SBT profile of class 3. Units U1 and U2 are characterized by a strong intrinsic variability of their mechanical properties. Since these units are the most involved in the soil-structure interaction mechanism of the Two Towers, a more detailed stratigraphic model is required at such depths, making use of the combined analysis of CPT parameter trends and paleosol stratigraphy.

The following **detailed geotechnical-stratigraphic model** can be defined based on CPT1.

- **Unit R** (approximately 0 - 4.5 m): anthropic fill, made of miscellaneous sediments with a variable grain-size distribution (clay/silty-clay locally sand/sandy-silt). This unit is characterized by a dark-brown colour and by the presence of numerous carbonaceous traces and various archaeological remains.
- **Unit U1** (approximately 4.5 - 16 m): alternation of clayey silt and silty clay horizons that vary in colour (from light hazelnut to dark brown), thickness (from half a meter to several meters), and stratigraphic position. This unit includes a succession of paleosols producing high scatter and increase with depth in the K_G* parameter (Fig. 9). Especially in its lower part, K_G* values are consistently above the threshold value, suggesting a significant influence of post-depositional processes. The alternation of weakly and highly pedogenized horizons also produces a remarkable scatter in mechanical properties. The subdivision of unit U1 into the following subunits is therefore necessary for accurate characterization.

The profiles of q_t and f_s, between 4.5 m and 9.2 m (**unit $U1_a$**) show marked and closely spaced peaks, with consequent variation of the mechanical properties (e.g., see the s_u profile) as a result of desiccated, thin (0.3-0.8 m) A_b horizons alternating with microstructured B horizons of variable thickness (Fig. 6). The most prominent peak of the succession, at 5.5 m depth, corresponds to the boundary between A_b and underlying B_k horizons of paleosol PH (Fig. 6).

Between 9.2 m and 11.5 m depth (**unit $U1_b$**), a marked reduction in mechanical and stress history parameters is clearly observed with respect to the overlying soil succession, together with a relatively uniform trend. This is consistent with the presence of a 2 m-thick, weakly pedogenized alluvial layer (B_w horizon, Fig. 6).

Between 11.5 m and 16 m (**units $U1_c$ to $U1_f$**), the alternation of A_b and B horizons (Fig. 6) has a clear fallout on the trend of the SBT_n profile, which drops from class 4 (typical of silty mixtures) in A_b to class 3 (typical of clays) in B. The A_b horizon of **unit $U1_c$**, between 11.5 and ~12.5 m (~1 m of thickness), underwent a remarkable aging process, as suggested by high OCR (~ 4.5, Fig. 9). The q_t and f_s profiles corresponding to the same horizon show an increase with depth and a peak at the interface between A_b and B_k with a decrement

in **unit U1$_d$.** A similar, but more marked trend can be observed in the second couple of A_b - B horizons (**units U1$_e$ and U1$_f$**).

- **Unit U2** (between 16 and 25.3 m) is characterized by an alternation of clayey silts and silty clays of green-grey colour. This unit shows a lower scatter in the s_u and OCR profiles, as a consequence of the limited and more spatially uniform influence of post-depositional processes with respect to unit U1. In particular, between 16 and 19.5 m depth (**unit U2$_a$**), the A_b horizons detected in continuous cores and laboratory tests are not visible in the CPT profiles, due to their limited thickness (0.10-0.20 m). The deposit between 19.5 and 25.3 m (**unit U2$_b$**) is characterized by an A_b horizon whose thickness varies laterally from few centimeters to more than 1 m (Fig. 6). The entire unit U2 is characterized by higher undrained shear strength compared to unit U1, with s_u values progressively increasing with depth toward the boundary with unit U3 (see Figure 9). Unit U2 also shows a lower scatter in the K_G* profile and, at the same time, a reduction in its average value relative to unit U1 (Fig. 9). Indeed, K_G* values are consistently below the threshold value, suggesting a lower influence of post-depositional processes.
- **Unit U3** (between 25.3 and 28 m - maximum investigated depth). This unit is made of normally consolidated (NC) alluvial clayey deposits (SBT_n 3), characterized by limited influence of post-depositional processes, together with a lower dispersion of soil properties and lower values of mechanical parameters (observe the s_u profile), compared to those of the overlying units. In agreement with their normally consolidated state, K_G* values lie well below the threshold and with very limited data dispersion.

Notably, the use of this refined geotechnical-stratigraphic model, instead of the preliminary one based on four units, has minimized the variability of the geotechnical parameters within each subunit, improving the accuracy in the estimation of representative parameters (i.e., their characteristic value and variation range). For instance, the standard deviation of s_u values, as estimated from CPT tests, shows a significant reduction for each identified subunit. Specifically, in Unit A_i (i = a to f), the percentage reduction ranges from 11% to 40%, while in subunits B_j (j = a, b) it ranges from 13% to 44%.

In Figure 10 A, the normalized dimensionless parameters – namely, the normalized cone resistance (Q_{tn}), the normalized friction ratio (F_r), the normalized pore pressure ratio (B_q), all defined in Table 1 – of CPTU2 are presented in terms of average value (continuous line) and standard deviation (dashed line) for all soil horizons. A_b and B_k horizons show similar values of average Q_{tn}, while B_w has a much lower value. The average value

of F_r decreases progressively from A_b to B horizons, while B_q and U_2 show a significant increment in B_w with respect to the other horizons (Fig. 10 A).

Figure 10 also shows the average values of the normalized parameters Q_{tn}, F_r, B_q and U_2 (the normalized excess pore water pressure, Table 1) of the three horizons, plotted on the Robertson's (1990) charts Q_t-F_r (B) and Q_t-B_q (C), on the Robertson's (2016) Q_{tn}-F_r chart (D) and on the Schneider et al.'s (2008) Q_{tn}-U_2 chart (E).

In the first Q_t-F_r chart (Fig. 10 B), the three coloured circles corresponding to the three horizons fall in SBT zone 3 (clays to silty clays), but from A_b to B_w horizon, the points move from the area characterized by higher OCR and aging toward the central area, corresponding to normally consolidated soils, consistently with their different post-depositional history. Similarly, in the Q_t-B_q chart (Fig. 10 C), A_b and B_k, are positioned closer than B_w to the boundary with SBT zone 4 (silt mixtures), toward soils with increasing OCR.

In the Robertson's (2016) Q_{tn}-F_r chart (Fig. 10 D), the three points plot in the CC zone (clay-like contractive soils) but, moving from A_b to B_w, the distance from the Lower Boundary Line (CD=60) decreases. This line, proposed by the same Author, based on observations of the behaviour of ideal overconsolidated fine-grained soils, marks the separation between contractive and dilative ideal soils at large shear strains. In the analysed case, the effects of post-depositional processes on soil microstructure appear to shift the points nearer to the boundary with the dilatative region, contrary to the expected contractive behaviour exhibited by cemented soils at large shear strains (Robertson, 2016). It is worth noting that, in the same chart, B_k and B_w are located very close to the boundary with the TC zone (transitional contractive soils), probably as a consequence of the higher silt content of these illuvial horizons with respect to A_b.

Chart (E) in Fig. 10 provides an alternative for investigating the presence of microstructurally strengthened soils, particularly in cases where the K_G* profile cannot be determined. In fact, microstructured soils, assuming comparable stress history and initial state to that of ideal soils, tend to exhibit high Q_{tn} values due to the increased strength and stiffness, combined with high positive U_2 values, which are indicative of contractive behaviour at large shear strains (Robertson, 2016).

6.2 From local calibration to the entire investigated area

The procedure applied to the previous CPT tests realized close to boreholed drillings, for which paleosol based stratigraphy was available, can be extended to a larger area using the other available CPT test data. In the Two Towers site, except for CPT1, the other field tests could not be calibrated using stratigraphic data from adjacent cores. Thus, lateral correlation of CPT profiles relied on vertical logs of OCR, as this parameter resulted

particularly suitable for recording the effects of pedogenic processes. In addition, SBT, q_t and f_s trends can provide supplementary evidence to support paleosol identification, as shown below.

A set of general guidelines is outlined for the potential identification of paleosol boundaries in other sites:
(a) The OCR trend in the A_b horizons shows a general increase with depth, but with a discontinuous profile characterized by alternating peaks and minor drops (as in $U1_c$ and U1e, Fig. 9); (b) the maximum value of the OCR profile is typically attained at the interface A_b - B_k, followed by a linear and rapid decrease (see 12.5 m and 14.8 m of depth in Fig. 9);
(c) fairly constant values of OCR (lower than those of the overlying horizons) characterize the B_w horizons (as $U1_b$ in Fig. 9);
(d) similar trends can be also observed in q_t and f_s profiles. In particular, more pronounced peaks characterize the f_s profile, together with a sharp plateau at the boundary between A_b and B horizons.
(e) the SBT profile shows a constant value across the B_w horizon (as in $U1_b$ and U3, Fig. 9), while in the pedogenized horizons (A_b and B_k) it increases with a scattered trend (as in U1c and U1e, Fig. 9).
This detailed analysis enabled to create the refined geotechnical model shown in sections X-X' and Y-Y' (Fig. 11). Lateral variations in mechanical behaviour, thickness and elevation of individual paleosol horizons were interpreted as local heterogeneities within each geotechnical unit. In the soil volume located beyond the influence of the tower foundations, however, the stratigraphic cross-sections show relatively small lateral variations (< 1m) in the depth and thickness of paleosols, possibly depending on inherited paleotopography (i.e. configuration of the ground surface at the time of soil formation), which in turn can be due to lateral variations in sedimentation rates, sediment compaction and soil erosion.

This methodological approach (Fig. 2) can potentially be extended to other coeval alluvial deposits, hosting paleosols with a similar degree of development (Inceptisols). Paleosol-bearing successions have been reported from other sectors of the Po Plain (Bruno et al., 2022 and references therein), from the Ganga plain (Gibling et al., 2005; Sinah et al., 2007), the Rhine-Meuse rivers in the Netherlands (Gouw & Hijma, 2022), and the Mississippi Delta (Aslan & Autin, 1998). It should be noted, however, that the typical triplet of horizons constituting the paleosols of the Po Plain is not always fully developped at the other sites. In the referenced studies, the physical properties of paleosol horizons (A_b, B_k, B_w) exhibit trends consistent with those observed in the subsoil of the Two Towers and show limited lateral variation. Consequently, a similar effect on the field

test responses is expected. The possible influence of the different composition of sediments draining different mountain basins is still unexplored, offering potential avenues for future research that could refine and generalize the proposed methodology.

7 Evidence of cumulative settlements below the Two Towers

In the soil volume below the foundations of the Two Towers, a noticeable deepening of subunits from U1a to U1f was observed (Figure 11), ascribable to soil compaction caused by the towers' weight.

Evidence of vertical deformation of paleosol profiles has proved extremely useful for estimating the cumulative settlement of the towers over their lifespan, a geotechnical issue otherwise affected by significant uncertainty. Typically, such estimations rely on historical sources (e.g., images, paintings, written documents) or the configuration of structural elements (e.g., the position of old doorsteps relative to the original ground level), rather than analytical approaches. A reliable estimation of average vertical settlement would require knowledge of the towers' original configuration relative to their surroundings, which is currently unknown.

Instead, evidence lies in the vertically deformed paleosols buried beneath the tower foundations, as shown in Figs. 6 and 11. These bent paleosols provide an approximate yet reliable estimate of cumulative settlement, calculated as the relative difference in depth between the paleosols buried beneath the foundations and the same horizons beyond the soil volume affected by the towers' load. The A_b horizon of P3, the shallowest continuous paleosol, was used as a reference level. For the Asinelli Tower, settlement was estimated by comparing the elevation of the A_b horizon of P3 in INCL1 and INCL2 (beneath the foundation, Fig. 11, top) and in SDH1 (outside the foundation, Fig. 11, bottom). Similarly, for the Garisenda Tower, the position of P3 was compared between ASS1 (beneath the foundation) and SPZ20 (outside, Fig. 11, top). Settlements of approximately 1.4 m and 1.2 m were estimated for the Garisenda and Asinelli Towers, respectively.

These values are consistent with the simplified analytical estimates by Bertolini et al. (2022a), which were 1.3 m for the Garisenda Tower and 1.7 m for the Asinelli Tower. However, the settlement deduced from paleosol deformation should be considered an approximate lower bound, as P3 is located ~3 m and ~2 m deeper than the foundation bases of the Garisenda and Asinelli Towers, respectively, and does not include the contribution of soil between the foundation base and the top of P3.

While paleosol deformation allows for the estimation of average vertical displacements, it does not enable the analysis of differential settlements, which can instead be directly inferred from the structure's inclination. The possible causes of the differential settlement of the Garisenda Tower have been debated in previous studies (Bertolini et al., 2022a; Marchi et al., 2022), which suggest that lateral heterogeneity of the subsoil—both in terms of thickness and mechanical properties—likely played a critical role. These two aspects are indeed interrelated, since anomalies in soil horizonation (e.g., in horizon thickness, depth from the founding plane), such as those inferred from the paleosol stratigraphy in Figure 6 (e.g., compare A_b of P3 in SPZ100 and SDH1), produces a non-homogenous horizontal distribution of mechanical parameters and thus different responses of the foundation soils under loading, inducing structure initial tilting and development of differential settlements over time.

Other potential factors that may have contributed to the initial tilting of the Garisenda—although not definitively proven—include an uneven distribution of structural loads, possibly due to the use of heterogeneous materials and rudimentary construction techniques, as well as the occurrence of plastic strains under partially drained loading conditions.

8 Conclusions

This paper outlines a methodological approach applied to the subsoil of the Two Towers in Bologna to interpret a 30 m-thick alluvial succession characterized by remarkable variability in mechanical properties, despite its relatively uniform texture.

An integrated stratigraphic-geotechnical approach was used. The stratigraphic model was developed through the analysis of six sediment cores and physical laboratory tests. Sedimentological analysis revealed the presence of a series of paleosols which testifies prolonged phases of subaerial exposure (leading to soil development) in a well-drained floodplain environment, interrupted by rapid sediment accumulation. Four paleosols, radiocarbon dated to the Late Pleistocene, are composed by three pedological horizons (A_b, B_k, B_w). Laboratory analyses indicate substantial transfer of carbonates from the exposed topsoil (A_b horizons) to the subsoil (B horizons) during each phase of pedogenesis. Leached carbonates accumulated in B_k horizons, creating cementation. Radiocarbon dating constrained the spatial correlation of paleosols.

In common geotechnical practice, stratigraphic models are typically derived from mechanical field tests supported by a limited number of boreholes, under the assumption that mechanical behaviour prevails over,

though remains correlated with, sediment composition. However, given the structural relevance of the investigated area and the complex subsurface conditions of intercalated microstructured horizons, a detailed stratigraphic analysis driven by a large number of borings is essential.

Standard SBT classifications from field investigations (particularly CPT tests) provided only a preliminary subdivision into geotechnical units. However, significant heterogeneities within these units hinder the definition of their representative mechanical parameters, requiring a more refined stratigraphic approach.

The combined use of paleosol stratigraphy and field tests enabled the identification of distinctive horizon features, allowing their potential recognition through calibrated field tests. A strategy was proposed using SBT, q_t and f_s and particularly OCR profiles obtained from CPT tests, to identify trends at paleosol horizon transitions. This approach enables tracing paleosols across the investigated area using standard field tests with minimal core coverage. Furthermore, changes in the thickness and elevation of subunits also allowed the estimation of the Two Towers' cumulative settlements over centuries, providing valuable data typically absent in similar studies.

This study highlights the effectiveness of an interdisciplinary stratigraphic-geotechnical approach and emphasizes the engineering potential of paleosol identification, potentially applicable to other similar alluvial settings.

Data Availability Statement

Some or all data, models, or code that support the findings of this study are available from the corresponding author upon reasonable request.

References

Amorosi A., Bruno L., Campo B., Di Martino A., Sammartino I. 2021. Patterns of geochemical variability across weakly developed paleosol profiles and their role as regional stratigraphic markers (Upper Pleistocene, Po Plain). Palaeogeography, Palaeoclimatology, Palaeoecology, **574**. DOI: 10.1016/j.palaeo.2021.110413

Amorosi A., Bruno L., Rossi V., Severi P., Hajdas I. 2014. Paleosol architecture of a late quaternary basin–margin sequence and its implications for high-resolution, non-marine sequence stratigraphy. Global and Planetary Change, **112**: 12–25. doi:10.1016/j.gloplacha.2013.10.007.

Amorosi A., Rampello S. 1998. The influence of natural soil structure on the mechanical behaviour of a stiff clay. *In* Proc. Int.Symp. Geotech. Hard Soils – Soft Rocks, Naples, **1,** pp. 395–402.

Aslan A., Autin W.J. 1998. Holocene flood-plain soil formation in the southern lower Mississippi Valley: Implications for interpreting alluvial paleosols. GSA Bulletin, **110**(4): 433–449. https://doi.org/10.1130/0016-7606(1998)110<0433:HFPSFI>2.3.CO;2

ASTM D7400M-19. 2019. Standard Test Methods for Downhole Seismic Testing.

Baxter C.D., Mitchell J.K. 2004. Experimental study on the aging of sands. Journal of Geotechnical and Geoenvironmental Engineering **130**(10): 1051-1062. doi: 10.1061/(ASCE)1090-0241(2004)130:10(1051).

Berisavljević D., Berisavljević Z. 2018. Determination of the presence of microstructure in a soil using a seismic dilatometer. Bulletin of Engineering Geology and the Environment, **78**(3). https://doi.org/10.1007/s10064-018-1234-5

Bertolini I., Marchi M., Gottardi G. 2022a. Learning from a Well-documented Geotechnical Cold Case: The Two Towers of Bologna, Italy. International Journal of Architectural Heritage. **17(10)**. https://doi.org/10.1080/15583058.2022.2057828

Bertolini I., Marchi M., Tonni L., Gottardi G., Bruno L., Amorosi A. 2022b. CPT data interpretation for an improved characterization of the paleosol stratigraphy in the Po River valley, Italy. Cone Penetration Testing, 1st edition, CRC Press, eBook ISBN9781003308829.

Bruno L., Marchi M., Bertolini I., Gottardi G., Amorosi A. 2020. Climate control on stacked paleosols in the Pleistocene of the po basin (northern Italy). Journal of Quaternary Science, **35**(4): 559–71. https://doi.org/10.1002/jqs.3199

Bruno, L., Campo, B., Hajdas, I., Hong, W. and Amorosi, A. (2022) Timing and mechanisms of sediment accumulation and pedogenesis: insights from the Po plain (northern Italy). Palaeogeogr. Palaeoclimatol. Palaeoecol., 591, 110881.

Buffardi C., Minderhoud P.S.J., Mandolini A. and Ruberti D. (2025) Characterizing Holocene sediments for assessing coastal-deltaic subsidence: the role of cone penetration tests and geomechanics. Front. Earth Sci. 13:1585388. doi: 10.3389/feart.2025.1585388

584 Burland J.B. 1990. On the compressibility and shear strength of natural clays. Géotechnique, **40(3):** 329-378.
585 https://doi.org/10.1680/geot.1990.40.3.329

586 Campo B., Bruno L., Amorosi A. (2023). Sedimentary facies characterization through CPTU profiles: An
587 effective tool for subsurface investigation of modern alluvial and coastal plains. Sedimentology, 70: 1302-
588 1327. doi: 10.1111/sed.13079

589 Cotecchia F., Chandler R.J. 1997. The influence of structure on the pre-failure behaviour of a natural clay.
590 Géotechnique, **47**(3): 523-544. https://doi.org/10.1680/geot.1997.47.3.523.

591 Cruz N., Rodrigez C., Viana da Fonseca A. 2012. Detecting the present of cementation structures in soils,
592 based in DMT interpreted charts. In: Couthino, Mayne (eds) In geotechnical and geophysical site
593 characterization. Taylor and Francis group, London, pp 1723–1728. ISBN 978-0-415-62136-6

594 Curzi P.V., Tonni L., Gottardi G., Mandanici E., 2017. High resolution sedimentological and geotechnical
595 characterization of the Late Quaternary deposits in the Italian central Adriatic coast (Tronto River mouth).
596 Engineering Geology, **220:** 219-233, https://doi.org/10.1016/j.enggeo.2017.02.007.

597 Demko T.M., Currie B.S., Nicoll K.A. 2004. Regional paleoclimatic and stratigraphic implications of paleosols
598 and fluvial/overbank architecture in the Morrison Formation (Upper Jurassic), Western Interior, USA.
599 Sedimentary Geology, **167**(3–4): 115–135. https://doi.org/10.1016/j.sedgeo.2004.01.003

600 Dunn R.L., Mitchell J.K. 1984. Fluid conductivity testing of fine-grained soils. Journal of Geotechnical and
601 Geoenvironmental Engineering ASCE, **110**(11): 1648–1665. https://doi.org/10.1061/(ASCE)0733-
602 9410(1984)110:11(1648).

603 El Howayek A., Bobet A., Santagata M. 2017. Geologic origin effects on mineralogy, index properties and
604 fabric of a fine-grained carbonatic deposit. Engineering Geology, **216**: 108-121.
605 https://doi.org/10.1016/j.enggeo.2016.11.017

606 Giacomelli S., Zuccarini A., Amorosi A., Bruno L., Di Paola G., Martini A., Severi P., Berti M., 2023. 3D
607 geological modelling of the Bologna urban area (Italy). Engineering Geology, 324, art. no. 107242.
608 https://doi.org/10.1016/j.enggeo.2023.107242

Gibling M.R., Tandon S.K., Sinha R., Jain M., 2005. Discontinuity bounded alluvial sequences of the southern Gangetic Plains, India: aggradation and degradation in response to monsoonal strength. Journal of Sedimentary Research, **75**: 369-385. https://doi.org/10.2110/jsr.2005.029

Gouw M.J.P, Hijma M.P. 2022. From apex to shoreline: fluvio-deltaic architecture for the Holocene Rhine–Meuse delta, the Netherlands. Earth Surf. Dynam., **10**: 43–64. https://doi.org/10.5194/esurf-10-43-2022

Hauser L., Oberhollenzer S., Marte R., Schweiger H.F., Tschuchnigg, F. (2025). Characterization of microstructure of a postglacial deposit based on in situ testing, laboratory testing, and numerical analysis. Journal of Geotechnical and Geoenvironmental Engineering, **151**(5). https://doi.org/10.1061/JGGEFK.GTENG-11985

Jefferies M.G., Davies M.P. 1993. Use of CPTu to estimate equivalent SPT N60. Geotechnical Testing Journal, ASTM, **16**(4): 458–468. http://dx.doi.org/10.1520/GTJ10286J.

Johnson D.L. 1998. Paleosols are buried soils. *In* L.R. Follmer, D.L. Johnson, J.A. Catt: Revisitation of Concepts in Paleopedology. Quaternary international, **51-52**: 7.

Ku T., Mayne P.W. 2013. Yield stress history evaluated from paired in-situ shear moduli of different modes, Engineering Geology, **152**(1): 122-132. https://doi.org/10.1016/j.enggeo.2012.11.001

Kulhawy F.H., and Mayne, P.W. 1990. Manual on Estimating Soil Properties for Foundation Design. Electric Power Research Institute EL-6800, Project 1493-6, Electric Power Research Institute, Palo Alto, California.

Leroueil S. 1992. A framework for the mechanical behaviour of structured soils, from soft clays to weak rocks. *In* Proc.US-Brazil NSF Geotechnical Workshop on Applicability of Classical Soil Mechanics Principles to Structured Soils, Belo Horizonte, pp. 107–128.

Leroueil S., Hight D.W. 2003. Behaviour and properties of natural soils and soft rocks. In "Characterisation and Engineering Properties of Natural Soils", Tan et al (eds). ISBN 90 5809 537 1

Leroueil S., Vaughan P.R. 1990. The General and Congruent Effects of Structure in Natural Soils and Weak Rocks, Géotechnique, **40**: 467-488. http://dx.doi.org/10.1680/geot.1990.40.3.467.

Ltifi M., Abichou T., Tisot J.P. 2014. Effects of Soil Aging on Mechanical and Hydraulic Properties of a Silty Soil. Geotechnical and Geological Engineering, **32 (4)**: 1101-1108. DOI: 10.1007/s10706-014-9784-1

635 Lunne T., Robertson P.K., Powell J.J.M. 1997. Cone penetration testing in geotechnical practice. Blackie
636 Academic, EF Spon/Routledge Publishing, New York, 312 pp. DOI: 10.1007/s11204-010-9072-x

637 Marchi M., Bertolini I., Gottardi G. 2022. A geotechnical insight into the soil-foundation system of the Two
638 Towers of Bologna, Italy. In: Geotechnical Engineering for the Preservation of Monuments and Historic Sites
639 III, CRC Press, London. http://dx.doi.org/10.1201/9781003308867-46.

640 Marchi M., Bertolini I., Gottardi G., Amorosi A., Bruno L. 2019. From geological and historical data to the
641 geotechnical model of the Two Towers in Bologna (Italy). In Proc. 17th European Conference on Soil
642 Mechanics and Geotechnical Engineering, ECSMGE 2019, Reykjavik, 1-6 September. DOI
643 10.32075/17ECSMGE-2019-0269

644 Mayne P.W., Peuchen J. 2018. Evaluation of CPTU Nkt cone factor for undrained strength of clays. In Cone
645 Penetration Testing 2018. The Netherlands: Delft University of Technology, pp. 423–429. eBook ISBN
646 9780429505980.

647 McCarthy P.J., Plint A.G. 1998. Recognition of interfluve sequence boundaries: Integrating paleopedology
648 and sequence stratigraphy. Geology, **26(5)**: 387-390. https://doi.org/10.1130/0091-
649 7613(1998)026<0387:ROISBI>2.3.CO;2

650 McCarthy P.J., Plint A.G. 2003. Spatial variability of palaeosols across Cretaceous interfluves in the Dunvegan
651 Formation, NE British Columbia, Canada: palaeohydrological, palaeogeomorphological and stratigraphic
652 implications. Sedimentology, **50(6):** 1187-1220. https://doi.org/10.1111/j.1365-3091.2003.00600.

653 Mitchell J.K., Soga K. 2005. Fundamentals of Soil Behaviour. 3rd Edition, John Wiley & Sons, Hoboken.

654 Mitchell, J.K. 1986. The Twentieth Terzaghi Lecture. Journal of Geotechnical Engineering, **112**(3): 255-289
655 doi:10.1061/(asce)0733-9410(1986)112:3(255)

656 Rampello S., Viggiani G.M.B. 2001. Pre-failure deformation characteristics of geomaterials – Invited
657 Discussion Leader Report. In Pre-Failure Deformation Characteristics of Geomaterials, 2nd IS-Torino 1999,
658 Balkema, Rotterdam, **2**: 1279-1289. ISBN 9058090752.

659 Robertson P.K. 2009. Interpretation of cone penetration tests - A unified approach. Canadian Geotechnical
660 Journal, **46**(11): 1337-1355. http://dx.doi.org/10.1139/T09-065.

661 Robertson P.K. 2015. Comparing CPT and Vs Liquefaction Triggering Methods. Journal of Geotechnical
662 Geoenvironmental Engineering, **141**(9). https://doi.org/10.1061/(ASCE)GT.1943-5606.0001338

663 Robertson P.K. 2016. Cone Penetration Test (CPT)-Based Soil Behaviour Type (SBT) Classification
664 System—An Update. Canadian Geotechnical Journal, **53**: 1910-1927. https://doi.org/10.1139/cgj-2016-0044.

665 Robertson P.K., 1990. Soil classification using the cone penetration test. Canadian Geotechnical Journal,
666 **27**(1): 151–158. doi:10.1139/t90-014.

667 Salvany J.M., Aguirre J. 2020. The Neogene and Quaternary deposits of the Barcelona city through the high-
668 speed train line. Geologica Acta, **18:** 1-19. DOI: 10.1344/GeologicaActa2020.18.10

669 Saye S.R., Lutenegger A.J., Santos J., Kumm B.P. 2013. Assessing overconsolidation ratios in soil with
670 piezocone: Referencing soil index properties. Journal of Geotechnical and Geoenvironmental Engineering,
671 **139**(7). https://doi.org/10.1061/(ASCE)GT.1943-5606.0000841

672 Scarciglia F., Sauer D., Zerboni A. 2023. Pleistocene paleosols of Italy: pedostratigraphy, genesis,
673 paleoclimate and geoarchaeology. Alpine and Mediterranean Quaternary **36**(2): 149-83.

674 Schmertmann J. H. 1991. The mechanical aging of soils. Journal of Geotechnical Engineering, **117**(9), 1288–
675 1330. https://doi.org/10.1061/(ASCE)0733-9410(1991)117:9(1288)

676 Schneider J.A., Randolph M.F., Mayne P.W., Ramsey N.R. 2008. Analysis of factors influencing soil
677 classification using normalized piezocone tip resistance and pore pressure parameters. Journal of Geotechnical
678 and Geoenvironmental Engineering, ASCE, **134**(11): 1569–1586. doi: 10.1061/(ASCE)1090-
679 0241(2008)134:11(1569)

680 Sinha R., Bhattacharjee P., Sangode S.J., Gibling M.R., Tandon S.K., Jain M., Godfrey D., 2007. Valley and
681 interfluve sediments in southern Ganga Plains, India: exploring facies and magnetic signatures. Sedimentary
682 Geology, **201**: 386-411. https://doi.org/10.1016/j.sedgeo.2007.07.004

683 Soil Survey Staff. 1999. Soil Taxonomy. A basic system of soil classification for making and interpreting soil
684 surveys, Agricultural Handbook. no. 436. Natural Resources Conservation Service, USDA: Washington, DC.

685 Soil Survey Staff. 2014. Keys to Soil Taxonomy, 12th ed. USDA-Natural Resources Conservation Service,
686 Washington, DC.

687 Srivastava P., Sinha R., Deep V., Singh A., Upreti N. 2018. Micromorphology and sequence stratigraphy of
688 the interfluve paleosols from the Ganga plains: a record of alluvial cyclicity and paleoclimate during the late
689 Quaternary. Journal of Sedimentary Research, **88**: 105–128. https://doi.org/10.2110/jsr.2018.10

690 Tentori D., Mancini M., Milli S., Stigliano F., Tancredi S. 2022. Compositional, micromorphological and
691 geotechnical characterization of Holocene Tiber floodplain deposits (Rome, Italy) and sequence stratigraphic
692 implications. Sedimentology, **69**(4): 1705-1737. https://doi.org/10.1111/sed.12969

693 Tsatskin A., Sandler A., Avnaim-Katav S. 2015. Quaternary subsurface paleosols in Haifa Bay, Israel: A new
694 perspective on stratigraphic correlations in coastal settings. Palaeogeography, Palaeoclimatology,
695 Palaeoecology, **426**: 285–296. https://doi.org/10.1016/j.palaeo.2015.03.018

696 UNI EN ISO 14688-1. 2018. Geotechnical investigation and testing - Part 1: Identification and description.

697 Yandong M.A., Jingbo Z., Rui L., Leipeng Y.I.N. 2018. Formation and movement of groundwater in the thick
698 loess-palaeosol sequences of the Chinese Loess Plateau. Pedosphere, **28**: 895–904.
699 https://doi.org/10.1016/S1002-0160(17)60419-3

700 Yenes M., Monterrubio S., Nespereira J., Casas D. 2020. Apparent overconsolidation and its implications for
701 submarine landslides. Engineering Geology, **264**. https://doi.org/10.1016/j.enggeo.2019.105375

702 TABLES AND CAPTIONS

703 ***Table 1: Main geotechnical properties (OCR, s_u and K_G*) and the Soil Behaviour Type Index (I_{cn}) as***
704 ***functions of the CPT parameters (Q_{tn}, F_r, U_2, B_q). n is a variable stress exponent depending on SBT_n (for***
705 ***fine-grained soil n~1); p_a is the atmospheric pressure (p_a ~ 100 kPa), k in the OCR formulation is the***
706 ***preconsolidation cone factor which varies between 0.2 and 0.5, with an average value of 0.33 (Lunne et al,***
707 ***1997), while in K_G* formulation, q_n is the net cone resistance and G_0 the small strain stiffness.***
708

Geotechnical parameter/index	Mathematical formulation and references	Variables and references
Soil BehaviourType Index **I_{cn}**	$I_{cn} = \sqrt{(3.47 - logQ_{tn})^2 + (logF_r + 1.22)^2}$ [Jefferies and Davies (1993), later revised by Robertson (2009)]	$Q_{tn} = [\frac{q_t - \sigma_{vo}}{p_a}](\frac{p_a}{\sigma'_{v0}})^n$ [Robertson (2009)] $F_r = \left[\frac{f_s}{(q_{t-\sigma_{vo}})}\right] * 100\%$ [Robertson (1990)]

Overconsolidation ratio $\boldsymbol{OCR}$	$OCR = k\left(\frac{q_t - б_{vo}}{б'_{vo}}\right) = k * Q_t$ [Kulhawy and Mayne (1990)]	
Undrained shear strength $\boldsymbol{s_u}$	$s_u = (q_t - б_{vo})/N_{kt}$	$N_{kt} = 10.5 - 4.6 * \ln(B_q + 0.1)$ [Mayne and Peuchen (2018)] $B_q = \frac{(u_2 - u_o)}{(q_t - б_{vo})}$ [Robertson (1990)]
Modified normalized small-strain rigidity index K_G*	$K_G^* = (\frac{G_0}{q_n})(Q_{tn})^{0.75}$ [Roberson, 2016]	$q_n = (q_t - \sigma_{vo})$
Normalized excess pore water pressure $\boldsymbol{U_2}$	$U_2 = \frac{(u_2 - u_0)}{б'_{vo}}$	

709

710

711

712 ***Table 2: Thickness of Late Pleistocene paleosols P1, P2, P3, PH and of their horizons as observed from***
713 ***cores recovered during the 2016 campaign. Note that no C horizons were detected in the paleosol succession.***
714

Paleosol	Thickness (mm)	Horizons succession	A_b thickness (mm)	B_k thickness (mm)	B_w thickness (mm)
PH	240-380	A_b-B_k / A_b-B_k-B_w	80	140-265	0-133
P3	400-500	A_b-Bk-B_w	85-230	< 90	250
P2	180-260	A_b-B_k / A_b-B_w	75-140	111-156	20-191
P1	400-500	A_b-B_k	65-155	237-337	37-140

715

716 ***Table 3: Variation ranges and average values of the main physical properties of A_b, B_k and B_w horizons, as***
717 ***determined from laboratory tests.***

	Range of variations (%)			Average values (%)		
	A_b	B_k	B_w	A_b	B_k	B_w
Clay content (%)	25-54	15-61	14-38	39	29	25
Silt content (%)	36-65	41-61	32-80	49	51	58
Sand content (%)	1-25	12-34	3-30	9	24	13
Plasticity Index (%)	12-46	13-22	15-37	29	18	23
Organic matter (%)	1.2-5.2	1.1-3.2	1.0-2.8	2.5	1.7	1.6
Carbonate content (%)	0.4-19.6	0.9-68.1	10.5-37.4	6.5	26.3	26.2

LIST OF CAPTIONS:

Fig. 1: Mechanism of formation of multiple soil sequences in subsiding alluvial settings.

Fig. 2: (A) Flowchart illustrating the step-by-step methodological approach for paleosol stratigraphic identification. (B) Workflow illustrating the proposed methodology for developing a refined geotechnical-stratigraphic model. (C) Segment of core SDH1 from Ravegnana Square, showing paleosol horizons A_b and B_k between 15 and 20 m depth. (D) Close-up of a centimeter-thick carbonate concretion within a B_k horizon in core SDH1, observed at a depth of 17.65 m.

Fig. 3: (A) Aerial view of Ravegnana Square (Bologna) captured from the top of the Asinelli Tower, with a map inset showing Bologna's location in northern Italy. (B) The two medieval towers: Garisenda (left, shorter) and Asinelli (right, taller) (Copyright UniBo immagine).

Fig. 4: (A) Overview of the Bologna urban area and adjoining foothills, showing subsurface stratigraphy. The drainage basins and associated alluvial fan systems are also shown south of the city. (B) Subsurface stratigraphy to a depth of 300 meters, highlighting the predominance of fine-grained deposits in the uppermost 100 meters beneath Bologna city centre. (C) Detailed stratigraphy of Bologna city centre with closely spaced paleosol correlations within the top 30 meters (modified from Amorosi et al., 2014 and Bruno et al., 2020).

Fig. 5: (A) Field investigations carried out during the campaigns of 1975, 1995 and between 2000 and 2009. (B) Main investigations performed in the 2016 campaign, along with older boreholes (blue dots) and the traces of sections Z-Z', X-X' and Y-Y', represented in Figs. 6 and 11.

Fig. 6: Correlation of Pleistocene paleosols along Section Z-Z' (see Fig. 5 B), within the uppermost 20-m, mud-prone succession beneath the Two Towers in the Bologna city centre (modified from Bruno et al., 2020). Radiocarbon dated samples are marked by red dots, with ages indicated in calibrated years before present (cal BP).

Fig. 7: Casagrande charts of soil samples by horizon: A_b (A, 16 samples), B_k (B, 18 samples), and B_w (C, 17 samples). Plasticity chart in accordance with EN ISO 14688-2.

Fig. 8: Comparison of physical properties of samples from A_b, B_k and B_w horizons on soil classification triangles. In graph (A, 40 samples), black dotted lines illustrate reading directions for a sample with 10% clay, 60% silt, and 30% sand. Dot sizes represent the Plasticity Index (PI) in graph (B, 33 samples) and organic and carbonate content in graphs (C, 38 samples) and (D, 26 samples), respectively.

Fig. 9: Left: Paleosol stratigraphic log of core SDH1. From left to right: corrected cone resistance (q_t), sleeve friction (f_s); pore water pressure at cone shoulder (u_2) with the equilibrium pore water pressure characterized by an hydrostatic regime below the water table located at a depth of 5.6 m from the ground level(u_0); Soil Behaviour Type Index (I_{cn}) and the resulting Soil Behaviour Type (SBT) vs depth (Robertson, 2009). The last three columns show the undrained shear strength (s_u) profile, including spot data from pocket penetrometer measurements, Overconsolidation Ratio (OCR), and the modified normalized small-strain rigidity index (K_G) along with shear wave velocity v_s. The threshold value of 330, proposed by Robertson (2016) as boundary between ideal and microstructured soils, has been superimposed on the K_G* profile. The proposed geotechnical stratigraphy, divided into units and subunits, is overlaid on the parameter profiles.*

Fig. 10: (A) Average values (continuous black lines) and standard deviation (dashed black lines) of the normalized parameters Q_{tn}, F_r, B_q and U_2 from CPTU2 across the different soil horizons (A_b, B_k, B_w) identified in SPZ20. The same average values are displayed on Robertson (1990)'s Q_t-F_r (B) and Q_t-B_q (C) charts, Robertson (2016)'s Q_{tn}-F_r chart (D), and Schneider et al (2008)'s Q_{tn}-U_2 chart (E).

Fig. 11: Stratigraphic cross-sections X-X' (top) and Y-Y' (bottom) of the subsoil beneath the Two Towers (refer to Fig. 5 B for the section trace location), showing CPT profiles and paleosol stratigraphy derived from continuous coring. Continuous black lines indicate the boundaries of units and subunits, while dotted lines with "?" symbols mark areas where in situ tests are unavailable (e.g., beneath the Asinelli and Garisenda foundations) or where missing core intervals prevent precise identification of paleosol horizons.

Notation

B_q	Normalized pore pressure ratio
s_u	Undrained shear strength
F_r	Normalized sleeve friction
fs	Sleeve friction
G_0	Small strain stiffness
I_c	Soil Behaviour Type Index
k	Preconsolidation cone factor
K_G*	Modified normalized small-strain rigidity index
LL	Liquid limit
n	Stress exponent depending on SBT_n
NC	Normally consolidated soil
N_{kt}	Empirical cone factor
OC	Overconsolidated soil
OCR	Overconsolidation ratio
p_a	Atmospheric pressure
PI	Plasticity index
PL	Plastic limit
q_n	Net cone resistance
q_t	Corrected cone resistance
Q_{tn}	Normalized corrected cone resistance
SBT	Soil Behaviour Type
u_0	Equilibrium pore water pressure
u_2	Pore water pressure at cone shoulder
U_2	Normalized excess pore water pressure
v_s	Shear wave velocity
$б_v$	In situ total vertical stress
$б_v'$	In situ effective vertical stress

Figure 1

Click here to access/download;Figure;figure 1 old

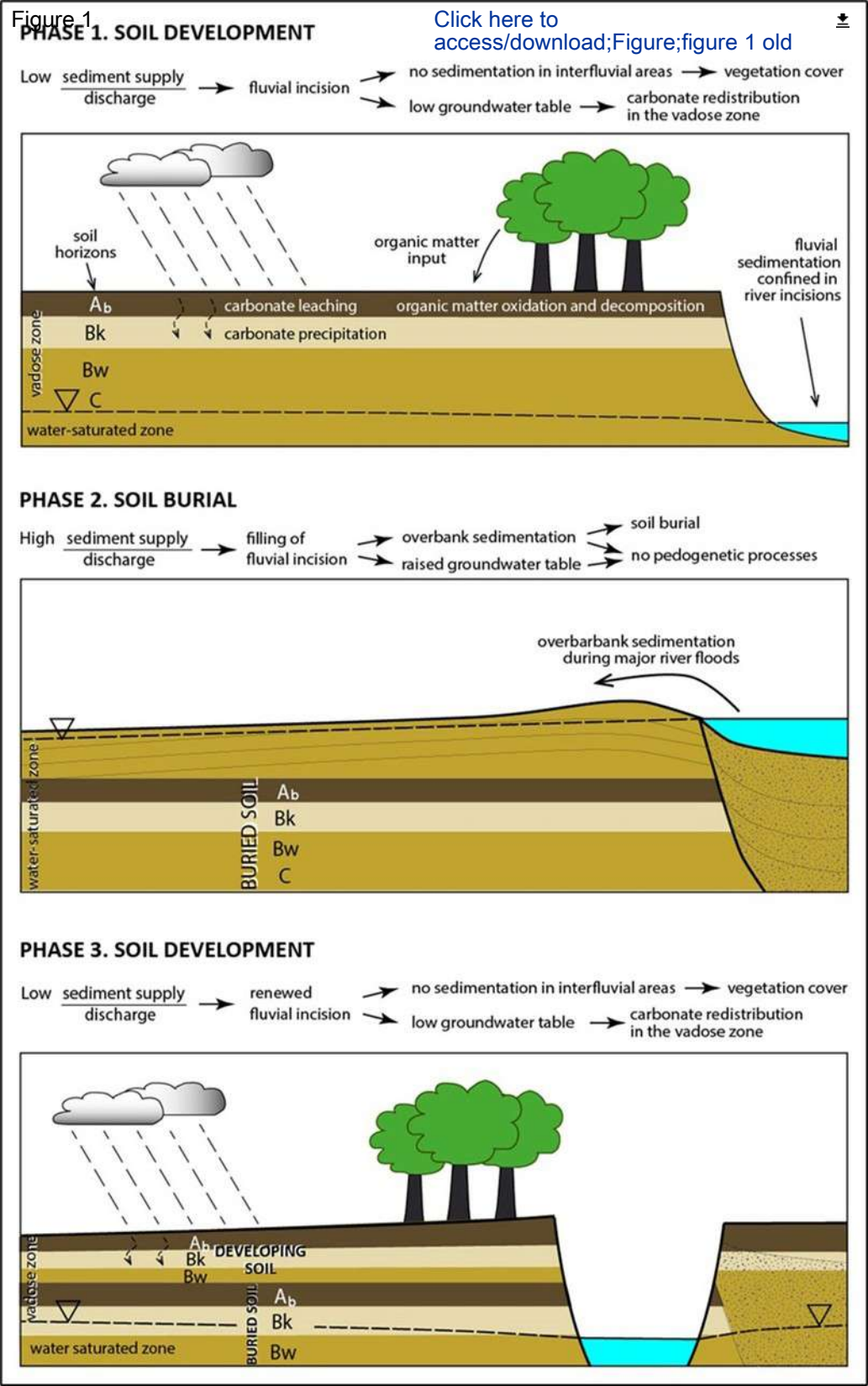

A

Paleosol identification

Continuous corings performed in the investi-gated area

Field core description

Quick tests on soil cores (Pocket Penetrometer, Torvane, soil reaction with hydrocloridic acid)

Laboratory tests on samples extracted from coring

Physical characterization of soil samples

Organic content(%)

Carbonate content(%)

Particle size distribution(%)

Atterberg limits

Radiocarbon dating

PALEOSOL STRATIGRAPHIC IDENTIFICATION

B

Geological Survey
(alluvial setting, paleosol predisposing factors)

In situ tests

n° 1 CPT

n° 1 Down-hole test or n° 1 Cross-hole test

n° 1 Continuous Coring

Geotechnical interpretation

Local calibration of field tests on coring analysis

SBT profile analysis

Identification of microstructured horizons: Kg*>330

Analysis of soil cores + Laboratory tests → **Paleosol identification** (Scheme A)

Paleosol-informed geotechnical model

Extension to the entire investigation area

Radiocarbon dating (lateral correlation of paleosol horizons)

Updated paleosol stratigraphy

Scattered CPTs over the area

OCR + q_t + f_s + SBT profiles analysis

Extended geotechnical- stratigraphic model

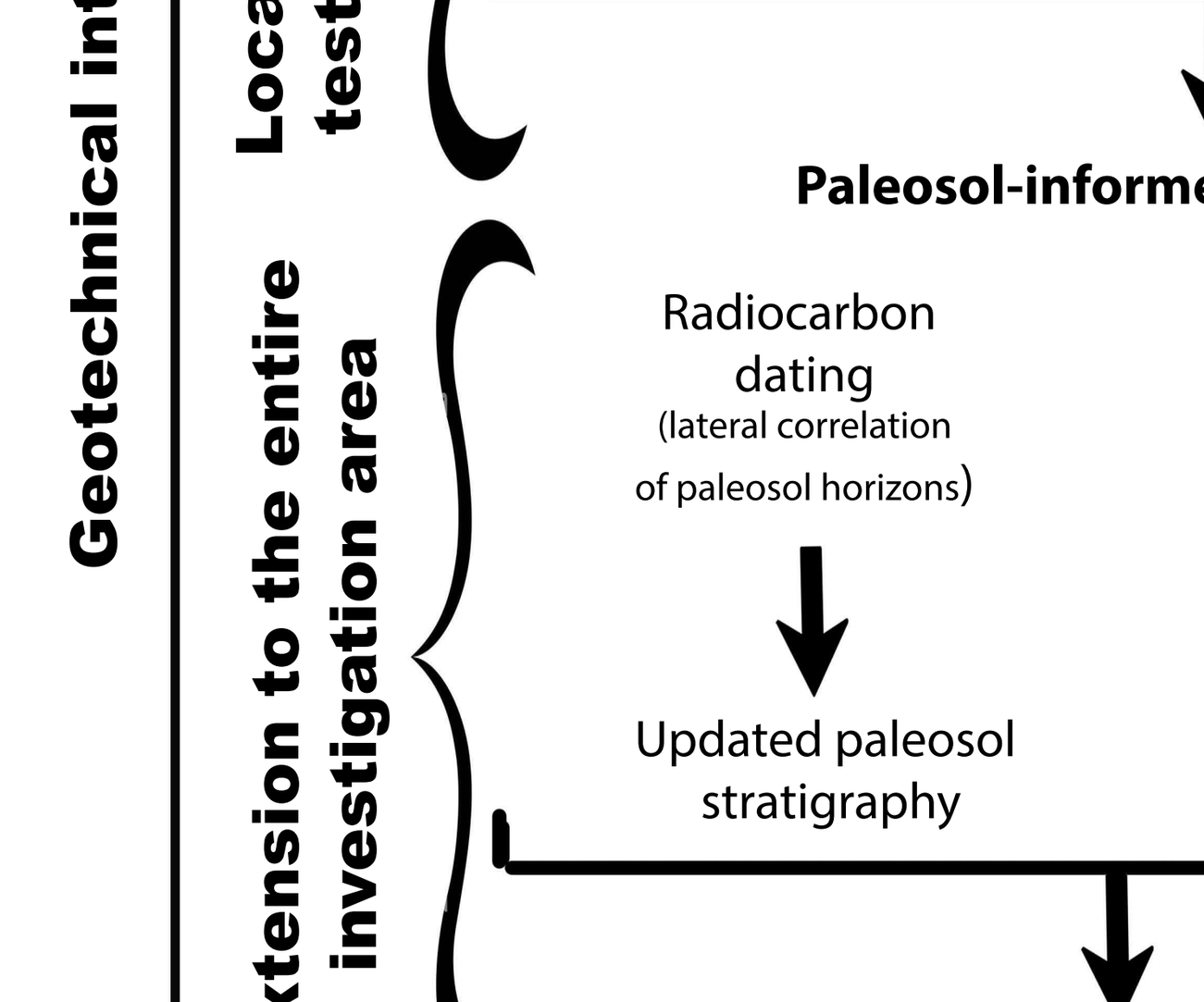

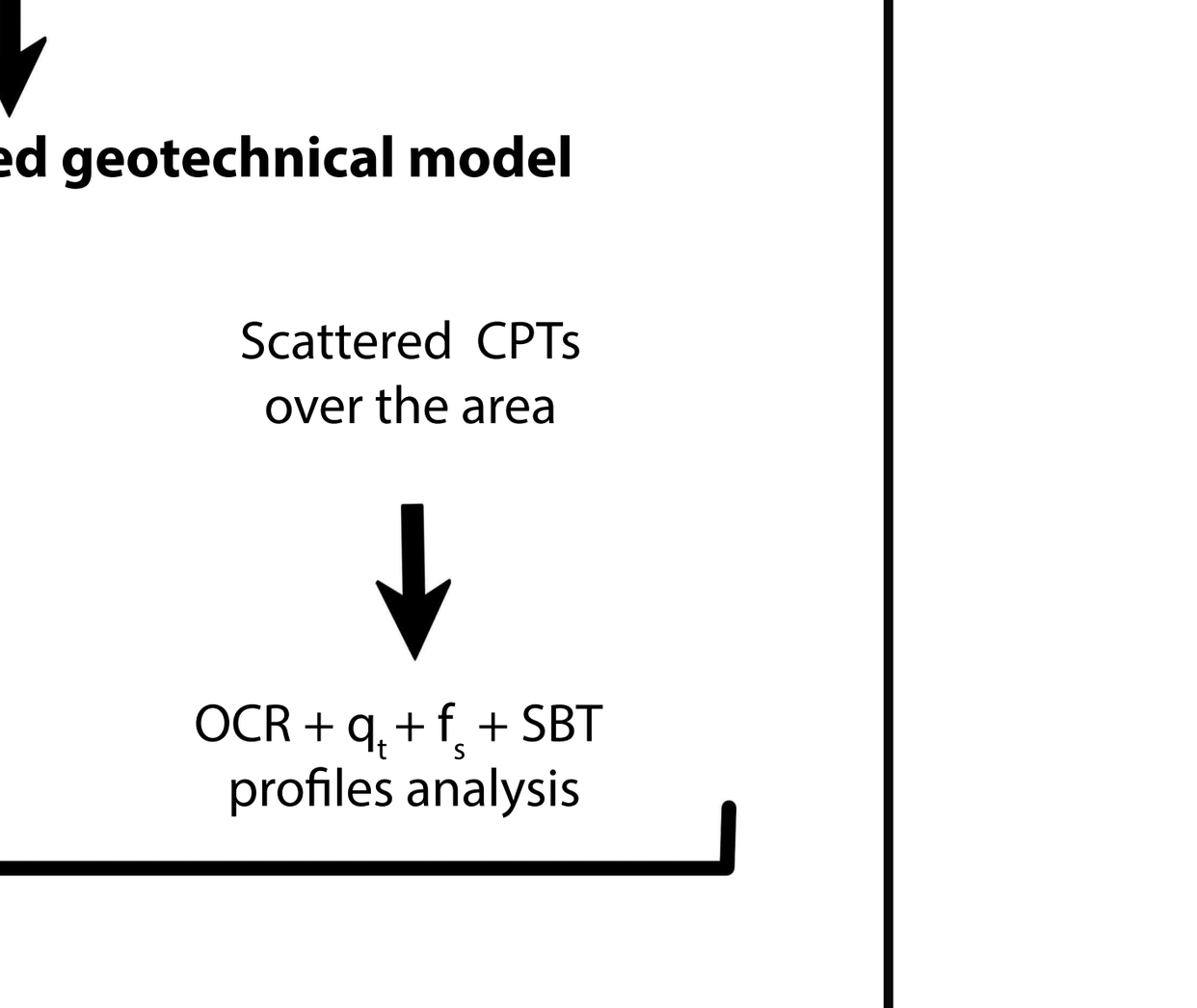

Figure 3

Click here to access/download;Figure;figure3 old 1.pdf

Figure 4

Click here to access/download;Figure;Figure_4.jpg

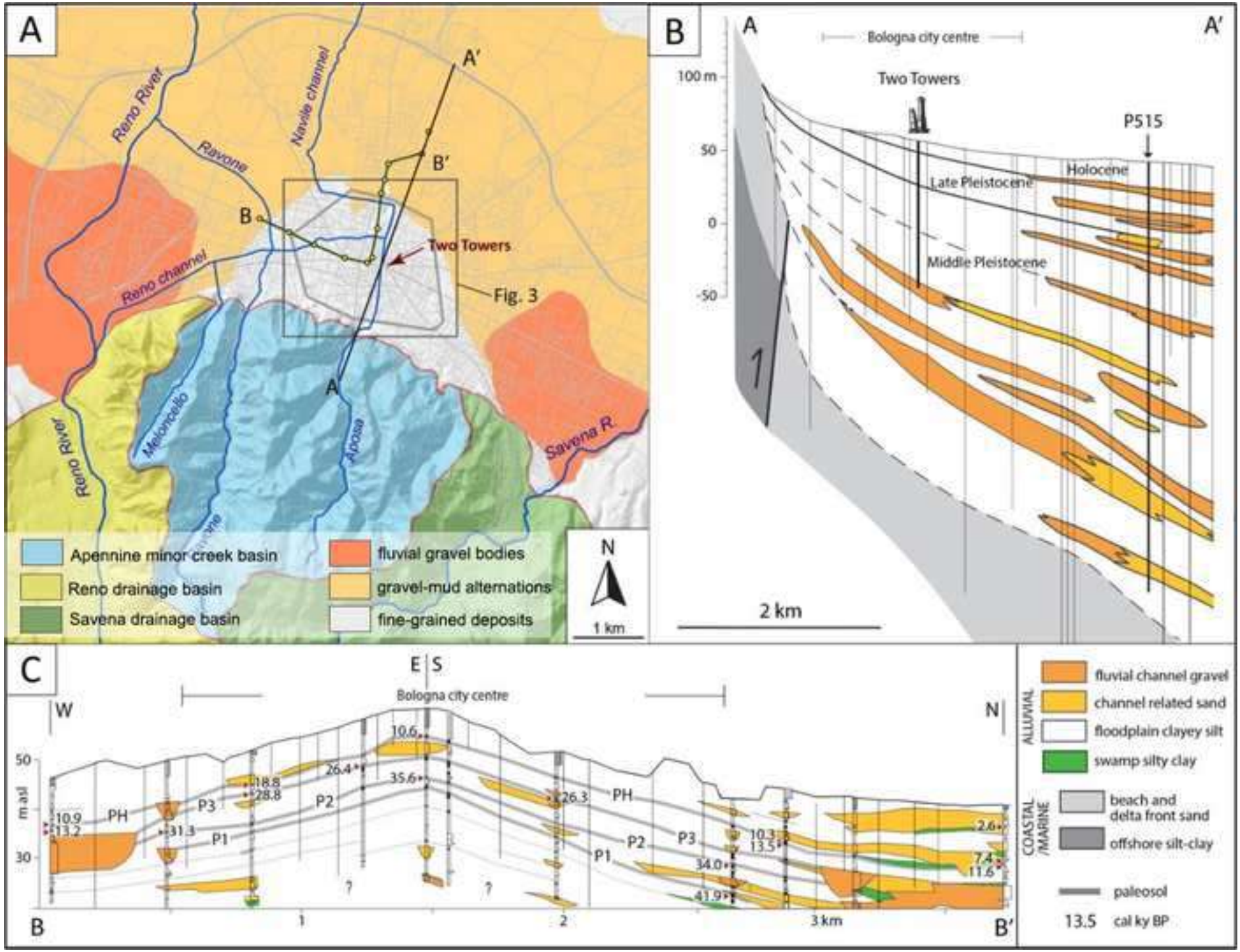

Figure 5

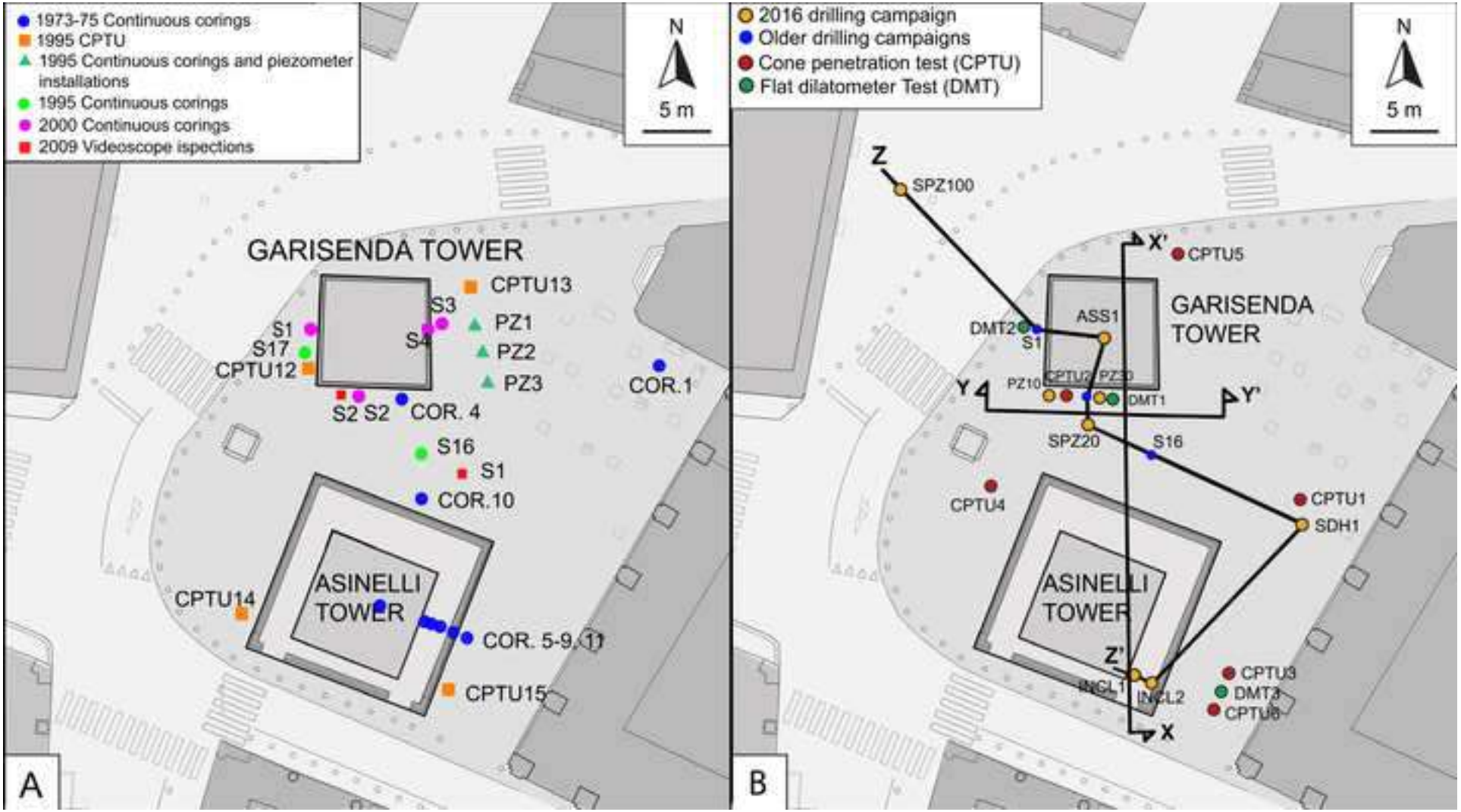

Figure 6

Click here to access/download;Figure;Figure_6.jpg

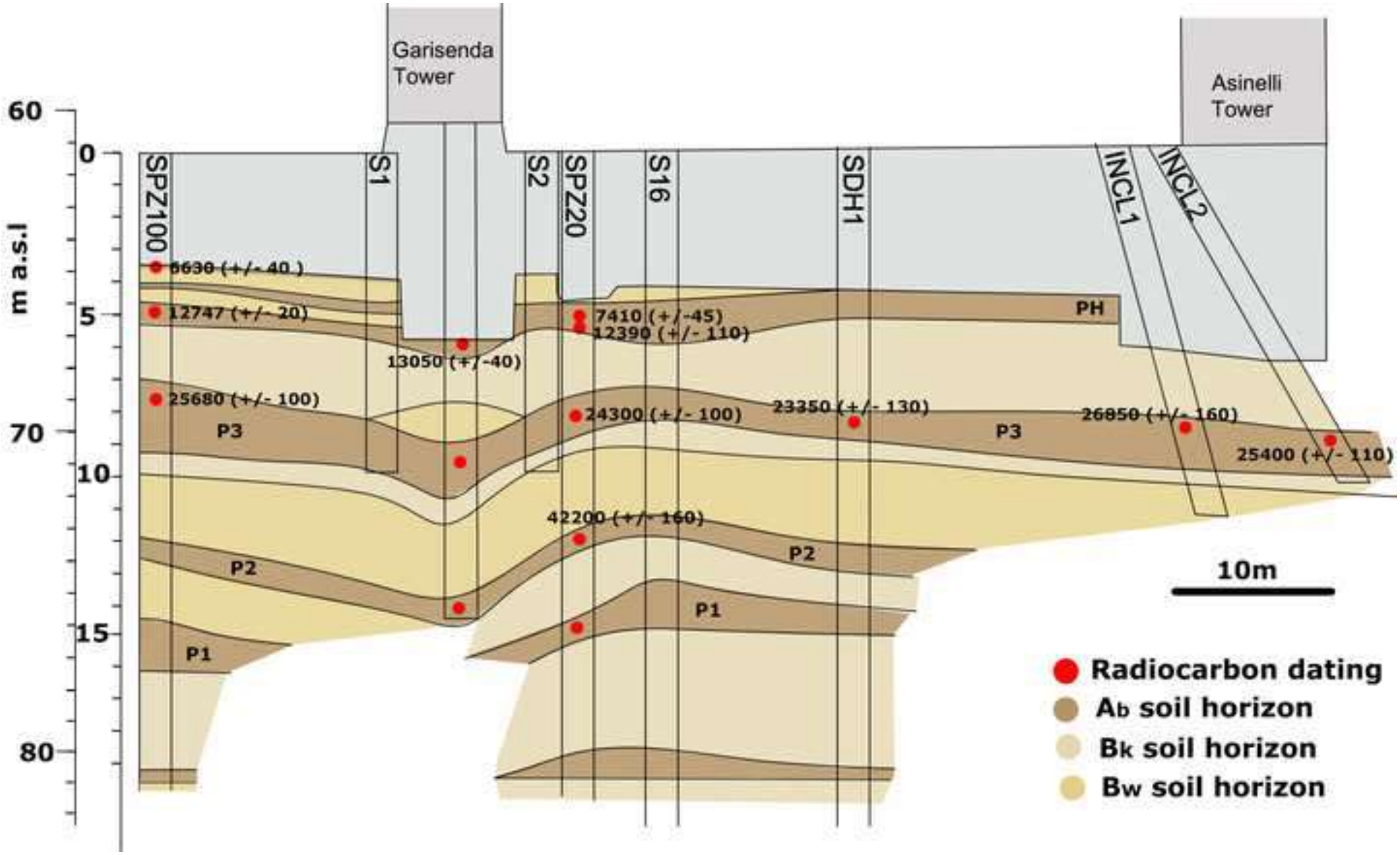

Figure7

Click here to access/download;Figure;figure7.pdf

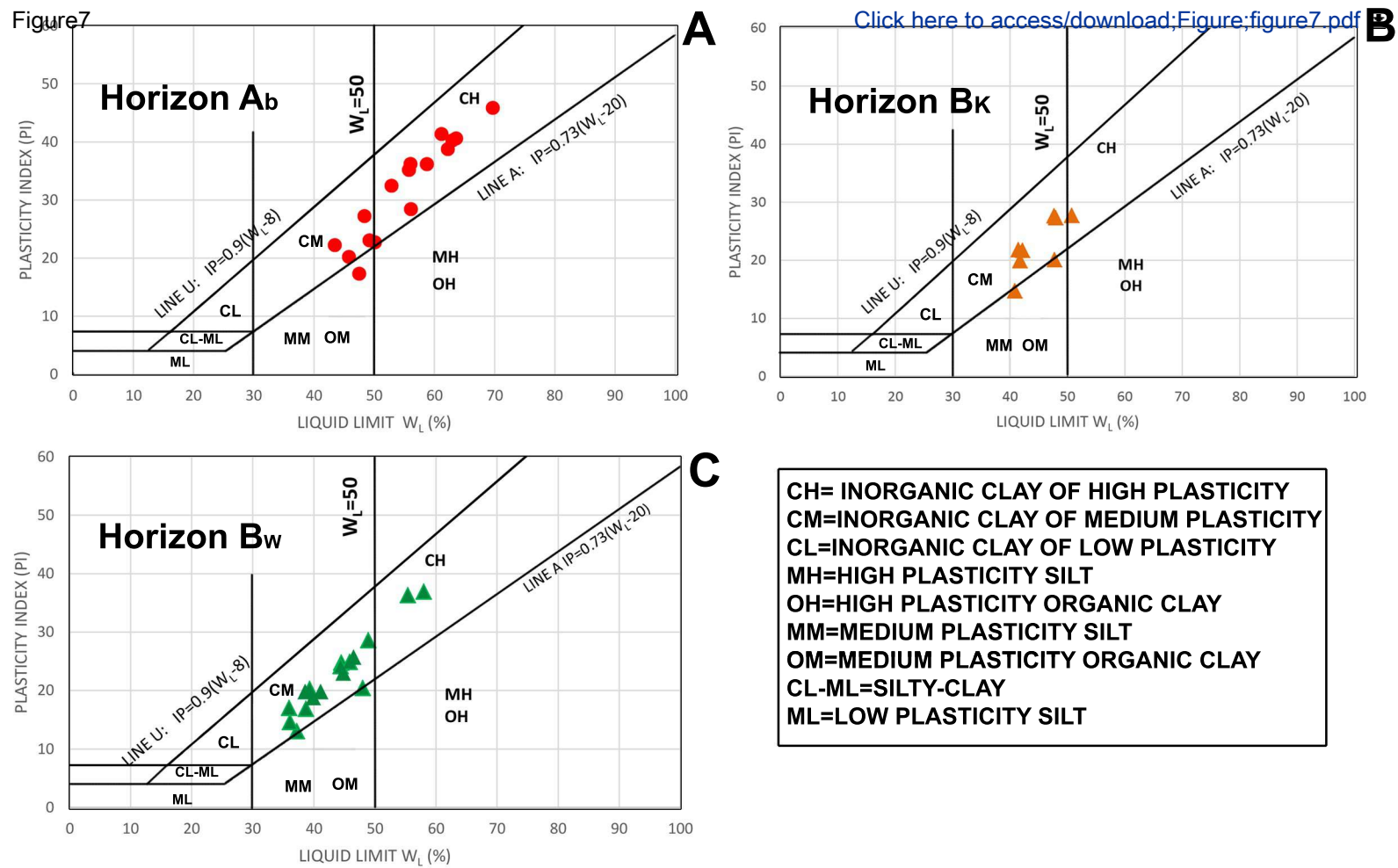

CH= INORGANIC CLAY OF HIGH PLASTICITY
CM=INORGANIC CLAY OF MEDIUM PLASTICITY
CL=INORGANIC CLAY OF LOW PLASTICITY
MH=HIGH PLASTICITY SILT
OH=HIGH PLASTICITY ORGANIC CLAY
MM=MEDIUM PLASTICITY SILT
OM=MEDIUM PLASTICITY ORGANIC CLAY
CL-ML=SILTY-CLAY
ML=LOW PLASTICITY SILT

Figure8

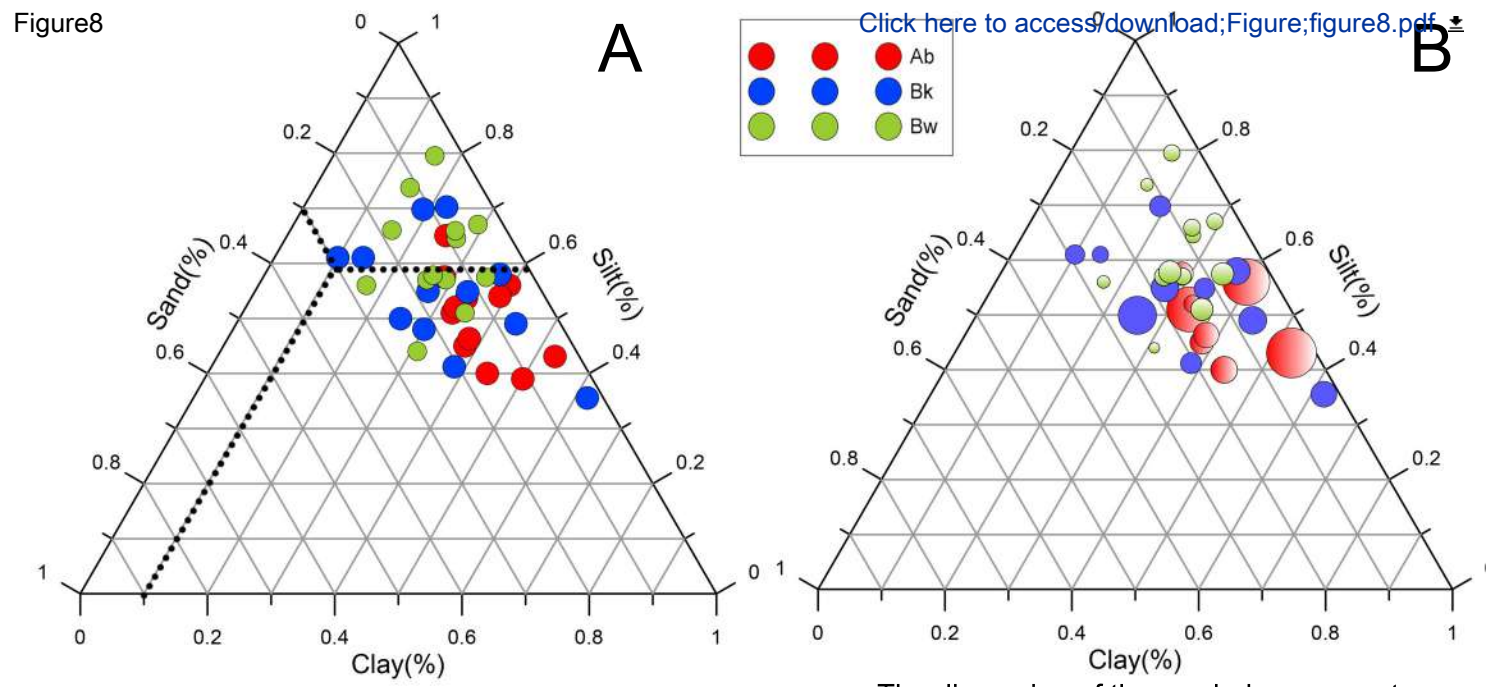

The dimension of the symbols represents the **Plasticity Index** (PI) value

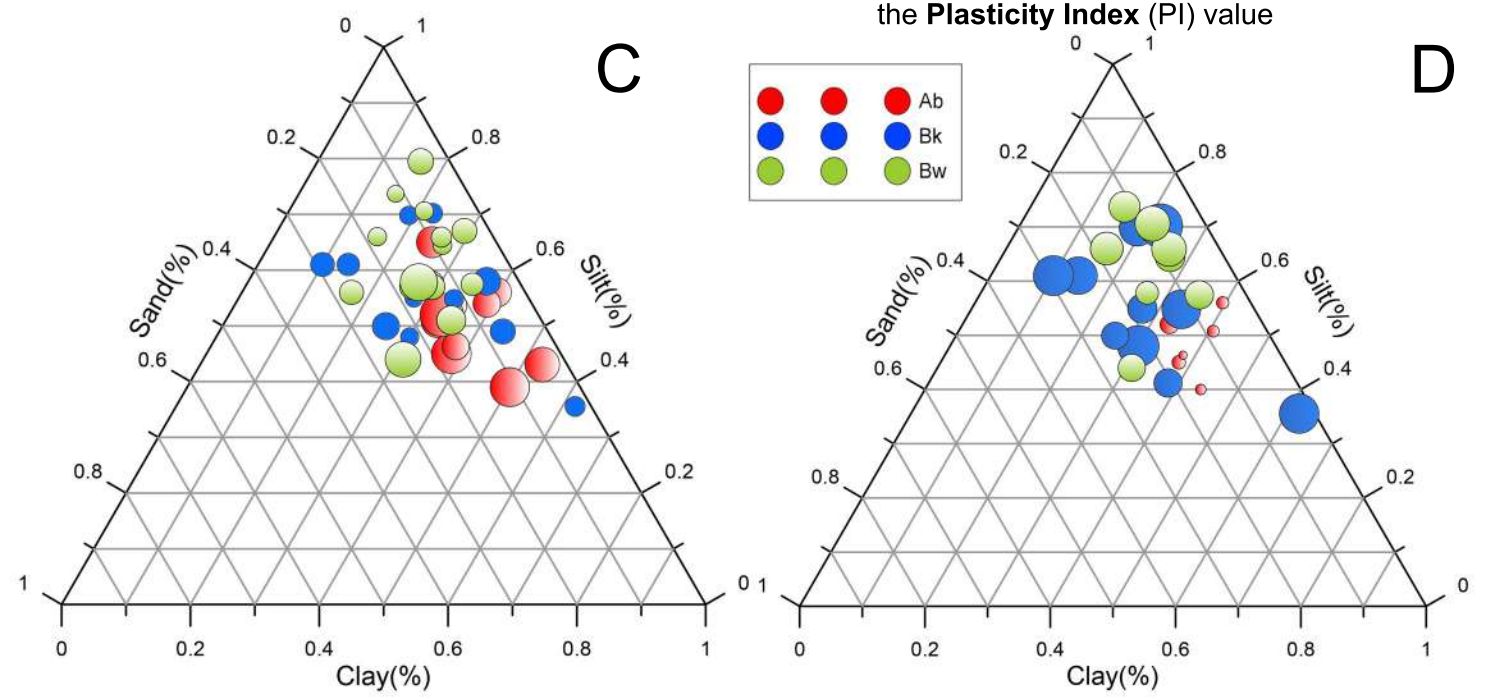

The dimension of the symbols represents the **organic content** (%) value

The dimension of the symbols represents the **carbonate content** (%) value

Figure9

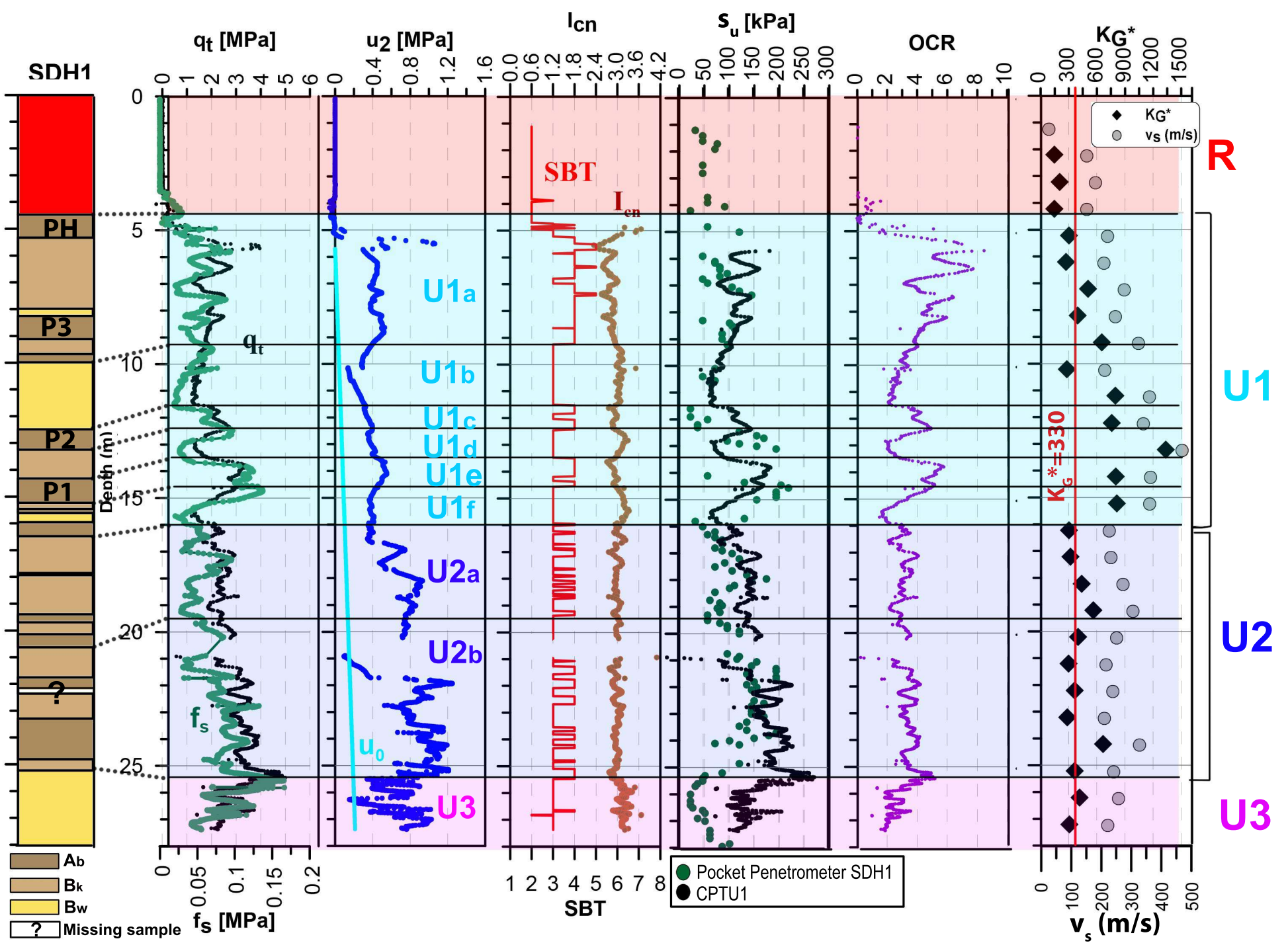

Figure10

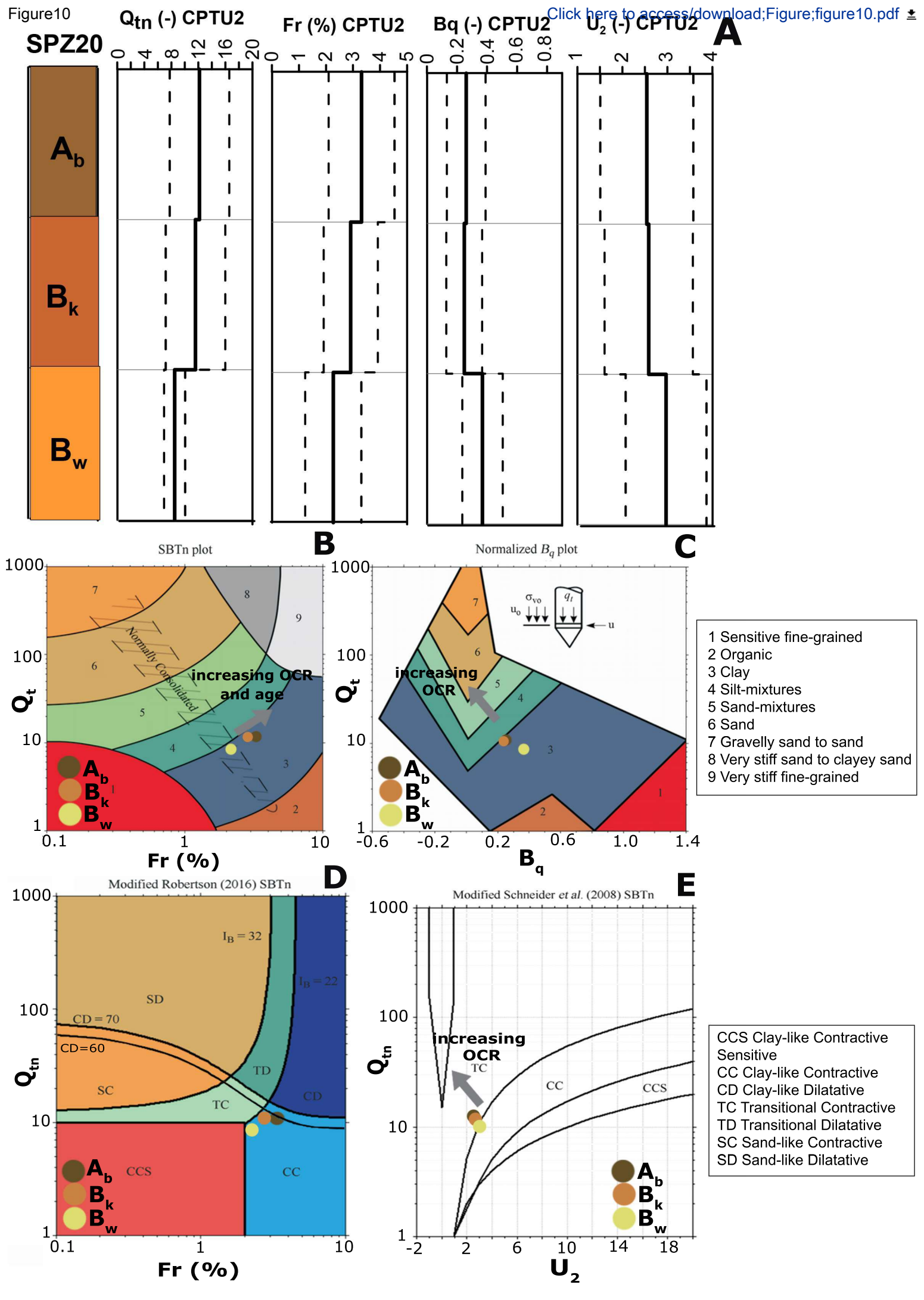

Figure11

Click here to access/download;Figure;figure11.pdf